SEMMELWEIS EGYETEM

DOKTORI ISKOLA

Ph.D. értekezések

3081.

KOVÁCSHÁZI CSENGER

Experimentális és klinikai farmakológia
című program

Programvezető: Dr. Szökő Éva, egyetemi tanár

Témavezető: Dr. Giricz Zoltán, tudományos főmunkatárs

Extracellular vesicles in hypercholesterolemia-induced cardiotoxicity and helium-induced cardioprotection

PhD thesis

Csenger Kovácsházi

Doctoral School of Pharmaceutical Sciences

Semmelweis University

Supervisor:
Zoltán Giricz, PhD

Official reviewers:
Zoltán Wiener, PhD
Gabriella Greskovics-Dobra, PhD

Head of the Complex Examination Committee:
Éva Szökő, PharmD, DSc

Members of the Complex Examination Committee:
Attila Oláh, PhD, Eszter Persa, PhD

Budapest
2024

Table of Contents

List of Abbreviations

AFM	atomic force microscopy
ANOVA	analysis of variance
ASC-GFP	apoptosis-associated speck-like protein containing a CARD domain fused by green fluorescent protein
ATP5A	ATP synthase lipid-binding protein
CM	cardiomyocyte
CVD	cardiovascular disease
CYR61	cysteine-rich angiogenic inducer 61
DNMT1	DNA (cytosine-5)-methyltransferase 1
ESCRT	endosomal sorting complexes required for transport
EV	extracellular vesicle
FDR	false discovery rate
GAPDH	glyceraldehyde-3-phosphate dehydrogenase
GO	gene ontology
HC	hypercholesterolemia
HeC	helium conditioning
HNRNPA1	heterogeneous nuclear ribonucleoprotein A1
IPC	ischemic preconditioning
LC-MS/MS	liquid chromatography bound tandem mass spectrometry
LFQ	label-free quantitation
mEV	medium-sized extracellular vesicle
Na-K-ATPase	sodium potassium ATPase
NRCF	neonatal rat cardiac fibroblast
NTA	nanoparticle tracking analysis
PBS	phosphate-buffered saline solution
PC	phosphatidylcholine
pEV	plasma extracellular vesicle
sEV	small extracellular vesicle
TBS	tris-buffered saline solution
TEM	transmission electron microscopy

1 Introduction

Our body is in a continuous dynamic balance that is called homeostasis. When this equilibrium is disturbed, biological mechanisms begin to function improperly. In response, the body initiates various compensatory processes to restore balance. However, if these stress-mechanisms fail to re-establish the original equilibrium, our body remains in a persistent imbalance. In result, biological processes will continuously malfunction, that is called as disease.

One of the most prevalent of these conditions is the group of cardiovascular diseases (CVDs). While its global burden has significantly declined in the last few decades [1] due to the extensive research and successful development of pharmacological and non-pharmacological therapies, it still remains the leading cause of deaths worldwide [2]. These data indicate that our current understanding on the pathomechanism resulting in the dysregulation of cardiovascular homeostasis is not yet complete. Gaining further insight into the regulation of harmful and compensatory mechanisms of the cardiovascular system could enable the development of novel therapies which help the body to restore healthy equilibrium.

1.1 Helium conditioning activates regenerative cardiac mechanisms

Biological processes associated with interventions to reduce cardiac injury in CVDs, and specifically in myocardial ischemia and reperfusion, are extensively studied to uncover the mechanisms underlying the innate stress response of the heart and to develop novel therapeutic interventions [3]. The most efficient so called cardioprotective intervention identified so far is ischemic preconditioning (IPC), consisted of a series of short ischemic periods applied to the myocardium before a prolonged ischemic event. This intervention significantly reduces the size of the necrotic tissue by activating self-defense molecular programs of the heart [4]. Other cardioprotective therapies, including ischemic conditioning on remote tissues or pharmacological treatments, have also been described with various underlying molecular pathways [3]. However, preclinical data represents discrepancies in efficacy of these interventions [5] and none have been successfully translated to clinical settings [3,6,7]. These results highlight that the molecular mechanisms of cardioprotection are not yet fully understood.

One of the cardioprotective interventions are inhalation of inert gases [8–10]. Specifically, the cardioprotective effect of helium have been demonstrated in multiple preclinical studies [11–14]. Helium conditioning (HeC) would be a non-invasive and clinically easily applicable cardioprotective intervention. Furthermore, as inert gas-induced cardioprotection is less studied so far, associated biological processes are not fully discovered. Further understanding of how HeC regulates myocardial functions could lead to the discovery of yet unknown cardioprotective signaling pathways and the development of more efficient interventions.

1.2 Hypercholesterolemia has direct cardiotoxic effects

A better understanding of cardiac homeostasis could be achieved by analyzing not only cardioprotective interventions, but cardiotoxic conditions. One significant harmful process contributing to the development of CVDs is the dysregulation of metabolic status of the body. The connection between high cholesterol levels and cardiovascular risk was demonstrated decades ago [15]; elevated cholesterol level is widely accepted as a principal risk factor for coronary artery disease. However, besides atherosclerosis, hypercholesterolemia (HC) alone has direct negative effects on the myocardium [16]. HC disrupts the physiological function of the heart, leading to impaired systolic and diastolic functions [17–19]. Additionally, it hinders cardioprotective interventions, such as IPC [20–22]. Despite these observations, the specific mechanisms underlying the direct cardiotoxic effect of HC are not well understood. Gaining a deeper understanding of the connection between metabolic status and CVDs is one of the possible directions to unravel the mechanisms responsible for the imbalances that results in CVDs.

1.3 Extracellular vesicles may lead to novel therapies and diagnostics in cardiovascular diseases.

Extracellular vesicles (EVs) are nano-sized membrane particles that are secreted by all cells and are present in intercellular spaces and biofluids. EVs were originally categorized by their biogenesis as exosomes, originated from the fusion of the multivesicular bodies with the plasma membrane, ectosomes, also known as microvesicles, which bud directly from the plasma membrane, and apoptotic bodies produced during programmed cell death [23]. However, recent findings have uncovered other secretory mechanism [24], and EV

subpopulations based on biogenesis cannot be experimentally separated or distinguished. Consequently, current guidelines classify EVs by size, source or isolation procedure used for sample preparation [25].

EVs carry a diverse array of molecular cargo including proteins, nucleic acids, lipid membrane components, and other metabolites. EV cargo are thought to be actively selected [26–28], though, passive stochiometric effects also contribute to the enrichment of specific compounds in EVs. As an example, miRNAs overexpressed in donor cells are similarly enriched in their EVs [29]. Therefore, EV composition reflects the phenotypic status of the donor cell. This phenomenon is driving efforts to use EVs from bodily fluids for diagnostic purposes. In the field of oncology, the first EV-based diagnostic products have been approved by the United States Food and Drug Administration [30,31], highlighting the yet unexploited possibilities in EVs.

Recipient cells uptake EVs where they bioactive cargo can induce phenotypic changes [32]. In this way, EVs establish paracrine and endocrine intercellular communication. Numerous studies aiming to utilize the functional effects of EVs to develop novel therapeutics are already in clinical phase according to *clinicaltials.gov* database. Specifically for CVDs, numerous preclinical studies demonstrates the potential of EVs as cardioprotective compounds [33,34]. However, our understanding on mechanisms driven by EVs is still limited, as they have been studied extensively in the last few decades only. Gaining insight into how EVs are dysregulated in CVDs or during cardioprotective interventions could reveal, novel information about the maintenance of cardiac homeostasis.

1.4 Extracellular vesicles in hypercholesterolemia

EVs play a role in both metabolic and cardiovascular diseases [35–37]. Furthermore, novel results demonstrating that EVs contribute to the connection of these disorders emerge. Davidson *et al.* have shown that type-II diabetes can inhibit EV-mediated cardioprotection [38]. Additionally, EVs derived from the plasma of high-fat-fed animals can exacerbate ischemic cardiac damage and induce cell death in cardiomyocytes (CM) [39,40]. These results suggest that connections between metabolic diseases and CVDs, which were previously hidden, could be revealed trough the analysis of EVs in HC.

HC may influence the cardiac tissue via blood EVs, which are derived from remote tissues, enter the circulation, and reach the myocardium where they modulate cellular functions, as well as via EVs derived from local cells, such as CMs. Therefore, to comprehensively investigate how HC contributes to CVD development via EVs, the analysis of both blood and cardiac-derived EVs is needed.

Numerous studies have evidenced that the number of circulating EVs is elevated in metabolic disorders [41–45]. Moreover, in familiar HC their amount is associated with the risk of future cardiovascular events [46,47]. Barrachina *et al.* analyzed the dysregulated proteome of circulating EVs in obesity and found that proteins involved in inflammation and coagulation are enriched in circulating EVs of obese patients [48]. Furthermore, they identified a reduction in the level of adiponectin, which is in relation with higher cardiovascular risk [49]. Similarly, analysis of the miRNA profile of circulating EVs in obese patients revealed that the targets of miRNAs upregulated in EVs in obesity are associated with inflammatory pathways [50]. These results suggest that EVs in HC may contribute to inflammation, which is one of the known mechanisms linking CVDs and HC [51]. However, how HC affects the metabolome of circulating EVs were yet not analyzed.

In contrast to circulating EVs, information on how HC affects the local EV communication of the myocardium is limited. An earlier study demonstrated that endothelial EVs of obese patients increased pro-fibrotic and pro-hypertrophic protein expression in CMs [52]. However, how HC modulates CM EV secretion is unknown. Therefore, to understand the connection between CVDs and HC, an in-depth analysis of CM EVs is necessary. CM-derived EVs regulate immune cell activation in multiple diseased conditions. EVs derived from CMs treated with angiotensin II to induce hypertrophy transform RAW264.7 murine macrophages to pro-inflammatory state [53,54]. Similarly, CM-derived EVs after myocardial infarction seem to induce macrophage polarization to a pro-inflammatory M1 phenotype [55,56]. Taking into account that proteomics and miRNA profile of circulating EVs in obesity also exhibit pro-inflammatory characteristics [48,50], it is plausible that HC results in the secretion of pro-inflammatory cardiac EVs.

1.5 Effect of helium conditioning on extracellular vesicles and cardiac fibroblasts

To understand how EVs play a role in the regulation of cardiac homeostasis, it is essential to investigate their role in cardioprotection. Our group has shown earlier that EVs play a pivotal role in ischemic conditioning [57]. Furthermore, HeC seems to regulate EV secretion as well. Weber *et al.* demonstrated in mice that HeC increased the number of Caveolin-3 rich circulating EVs [58]. Helium also increases EV secretion from murine neutrophils [59] and endothelial cells [60]. These results suggest that HeC may affect cardiac EV secretion that contribute to its regenerative mechanisms.

Cardiac tissue is composed of multiple cell types, including CMs, endothelial cells and cardiac fibroblasts (CFs) [61]. While CMs are responsible for the pump function of the heart, endothelial cells and CFs are crucial for maintaining the appropriate microenvironment and homeostasis for CMs. Additionally, they play significant roles in cardiac repair after myocardial infarction [62–65]. In our common work, Marek Jelemenský demonstrated that HeC promotes CF migration [66], which may be responsible for enhanced cardiac regeneration. As CFs can protect CM from cell death during myocardial infarction via paracrine factors [67–69], including EVs [70], we hypothesized that CFs might secrete EVs or other mediators that promote post-infarction cardiac regeneration. However, Jelemenský's work showed that pro-migratory effect of HeC cannot be transferred to naïve CFs from HeC-treated CFs via paracrine factors [66]. On the other hand, whether HeC indirectly activates endothelial cells via CFs, and how it regulates CF EV secretion has not been addressed.

1.6 Analysis of extracellular vesicles may reveal novel information on the pathophysiology of the heart

Considering these information, we aimed to investigate how EVs contribute to the maintenance of cardiac equilibrium. We addressed HC as a mechanism that dysregulate cardiac homeostasis and HeC that aims to alleviate cardiac stress. To gain deeper insight into blood-derived EVs in HC, we investigated the metabolomic profile of plasma-derived EVs (pEV) of rats fed with high-cholesterol chow, as it had not been previously addressed on circulating EVs. Furthermore, we performed in-depth analysis of CM s mall EVs (sEV) under HC conditions. In the context of HeC, we analyzed CF medium-sized EV (mEV) secretion and the effect of CF secretome on the function of endothelial cells.

2 Objectives

We hypothesized that HC dysregulates the composition of both circulating and cardiac-derived EVs contributing to the progression of CVDs. Furthermore, we hypothesized that HeC modifies EV secretion of CFs, which could contribute to its cardioprotective effect. By analyzing EVs in both cardiotoxic and cardioprotective mechanisms we aim to gain deeper understanding of the role of EVs in maintaining cardiac homeostasis. According to our hypotheses, we have established the following objectives:

1) **Analyze how HC modifies circulating EV metabolome:**
   EVs are composed of membrane lipids, inter- and transmembrane proteins and cargo of nucleic acids and other metabolites. As protein and miRNA content of circulating EVs in obesity was addressed earlier [48,50], here we aimed to extend our knowledge on how metabolic diseases affects EVs by analyzing their metabolite composition, including certain membrane lipids.
2) **Analyze the effect of HC on CM EV secretion:**
   Both circulating and local EVs can affect the myocardial homeostasis. However, how HC dysregulates CM EV secretion has not yet been analyzed. To gain insight into how HC contributes to CVD formation via EVs, we aimed to perform an in-depth analysis of CM EVs
3) **Analyze whether CM EVs induce inflammation in HC:**
   As circulating EVs seem to promote inflammation in HC [48,50] and HC-induced inflammation plays a role in CVD formation [51], we hypothesized that CM EVs play a role in such mechanisms. Therefore, we aimed to analyze the effect of CM EVs on immune cells.
4) **Analyze the effect of HeC on CF EVs:**
   HeC activates stress-adaptive mechanisms of the heart [13] and may affect EV secretion as well [58–60]. Previously, with Marek Jelemenský we demonstrated that HeC facilitates CF migration [66]. To investigate how HeC regulates cardiac EVs, we aimed to analyze its effect on CF EV secretion.

3 Methods

3.1 Treatment of hypercholesterolemic rats

Experiments on male Wistar rats were approved by the National Scientific Ethical Committee on Animal Experimentation and the Semmelweis University's Institutional Animal Care and Use Committee (project identification code: PE/EA/1912-7/2017; date of approval: November 2017) and all experiments were performed in accordance with the ARRIVE guidelines.

Hypercholesterolemic animal model was implemented as we described [71]:

"Male Wistar rats were fed either with standard (n = 11) or high cholesterol (n = 7) chow for 12 weeks. HC chow contained 2% cholesterol and 0.25% cholic acid. Animals were housed in a temperature (22 ± 2 °C)-, and humidity-controlled (50 ± 10%) room at a 12-h light/dark cycle and had free access to laboratory chow and drinking water ad libitum. After the 12-week period, the animals were anesthetized intraperitoneally with 60 mg/kg pentobarbital and their blood was collected from the abdominal aorta into Anticoagulant Citrate Dextrose-A vacuum tubes. Platelet-free plasma (PFP) was obtained by centrifugation twice with 2,500 ×g at 4 °C, for 15 min. as previously described[ref.: [72]*]. PFP samples were stored at -80 °C."*

3.2 Isolation of extracellular vesicles from rat plasma

Male Wistar rats were treated as described above, then platelet-free plasma samples were collected and used for pEV isolation according to the protocol described by Onódi *et al*. [73]. In brief, plasma samples were first loaded onto an iodixanol (Axis-Shield, Oslo, Norway) density gradient column, and density gradient ultracentrifugation was performed for 24 h at 120,000 × g at 4 °C. The gradients were separated to twenty equal-sized fractions. EV-rich fractions (fractions 8-10) were pooled and further isolated with size exclusion chromatography using a HiScreen Capto Core 700 column (GE Healthcare Life Sciences) using the Vezics system (vezics.com).

3.3 Metabolomics of rat plasma and plasma-derived extracellular vesicles

Metabolomics were performed by the Department of Laboratory Medicine, Laboratory of Mass Spectrometry and Separation Technology of Semmelweis University.

Plasma and pEV samples were analyzed using the same procedure. Equal amount (0.01 mL) of samples were analyzed with a Biocrates MxP Quant 500 kit (Biocrates AG, Innsbruck, Austria) according to the manufacturer's instructions, as we detailed earlier [71]. For the analytical procedure and data analysis, Biocrates MetIDQ software (version 7.13.11, DB109-Nitrogen-2850 Revision 31995, Base Version 109, Runtime version 1.8.0_181, Runtime architecture amd64; Biocrates A.G., Innsbruck, Austria) was used. Analytical system control and data acquisition were performed using Sciex Analyst (version 1.5.3).

Quantified data were analyzed using R programming language [74] as we described earlier [71]: *"Metabolites were excluded from the analysis if less than half of the measurements (< 7 for CTRL and < 4 for VEH) were below the limit of detection (LOD) in both groups independently for EV and plasma samples. For the analytes included, values below the LOD were imputed with a normal distribution around half of the LOD. For correlation analysis, metabolite types for which at least twelve plasma-EV measurement pairs were available were analyzed with linear regression model. For both linear regression and statistical analysis, data were log10 transformed."*

3.4 Culturing and hypercholesterolemic treatment of AC16 cardiac myocytes

AC16 human cardiomyoblast cells (CRL-3568; ATCC, Manassas, VA, USA) were cultured as we described earlier [71]:

"[Cells] were cultured in Dulbecco's Modified Eagle medium and Nutrient F12 1:1 mix (DMEM/F12) (Capricorn, Cat. no.: DMEM-12-A) supplemented with 12.5% heat-inactivated fetal bovine serum (FBS) (Corning, Cat. no.: 35-079-CV), 2 mM of L-glutamine (Corning, Cat. No.: 25-005.CI), 10mM of HEPES (N-2-hydroxyethylpiperazine- N-2-ethane sulfonic acid) (Gibco, Cat. No: 15630-056) and 1% Antibiotic-Antimiotic Solution (Corning, Cat. No.: A5955-100ML). Cells were kept at 37 °C in a 5% CO2/95% air environment and subcultured by trypsinization (TrypLE) (Gibco, Cat. No.: 12604-021) when cells reached 90% confluence."

For HC treatment, a total of 3.5 million cells were seeded into 175 cm^2 culture flasks. The day after seeding, culturing medium was replaced with fetal bovine serum (FBS)-free medium. For HC treatment, the medium was supplemented with Refeed® (Remembrane, Imola, Italy) hypercholesterolemic supplement. As vehicle, 3 µL/mL 96% ethanol was added to the medium. Cells were incubated for 48 hours with the treatment medium. After treatment, the supernatant was collected for sEV isolation, and the cells were trypsinized and counted using a hemocytometer. Viability was determined by Trypan blue (Cytiva, Cat. No.: SV3008401) staining. Samples were excluded from the analyses if viability did not reach 90%.

3.5 Oil Red O staining of AC16 cells

Oil red O staining of AC16 cells were performed as we described earlier [71]:

"AC16 cells were seeded on CELLview cell culture microscope slides (Greiner Bio-One, Austria) at a concentration of 20,000 cells / well. After 24 hours, the cells were treated with HC treatment solution, then cultured for another 48 hours at 37 °C in a CO_2 incubator. The cells were fixed in 10% neutrally buffered formalin, washed with ultrapure water and then with 60% isopropanol. The cells were then stained with Oil Red O solution (3 mg/mL) (Sigma, USA, Cat. No.: O0625-25G) for 10 minutes. This was followed by another wash with isopropanol followed by ultrapure water, and the nuclei were labeled with 1:1,000 dilution of DAPI (Cell Signaling Technologies, Danvers, MA, USA, Cat. No.: 4083S) for 1 minute, and the samples were covered with Prolong Gold (Thermo Scientific, Waltham, MA, USA) mounting medium and coverslips were applied. Samples were examined with a Leica SP8 confocal microscope. Oil Red O dye was excited at 552 nm and the emitted fluorescence was detected in the range of 645-767 nm."

3.6 Isolation of extracellular vesicles from cell culture supernatant

EVs from in vitro cell culture supernatant were isolated using differential centrifugation, as we described earlier [71]:

"Culturing medium was collected in 50 mL centrifuge tubes and EVs were isolated using differential centrifugation. Cell supernatants were centrifuged at 300×g at 4 °C for 10 min (Hettich Universal 320R; Rotor type: 1494 with Hettich 1427 adaptor). Then supernatants were centrifuged at 2,500 × g at 4 °C for 5 min (Hettich Universal 320R;

Rotor type: 1494 with Hettich 1427 adaptor). The supernatants were transferred into 50 mL centrifuge tubes (Herolab Cat. no.: 253211) and centrifuged at 13,500 × g at 4 °C for 40 min (Hermle Z326K; Rotor type: 220.78 V20.).”

To isolate mEVs, supernatant after the last centrifugation step was resuspended in 200 µL phosphate-buffered saline (PBS). To isolate sEVs, the protocol continued as we described [71]:

“[Supernatants] were transferred into ultracentrifuge tubes (Beckman Coulter, Cat. no.: 326823) and centrifuged at 174,900 × g at 4 °C for 3 h using an ultracentrifuge (Optima XPN-100; Rotor type: SW32Ti with adaptor 129.7). Pellets were resuspended in 120 µL of phosphate-buffered saline (PBS) or in 120 µL of Tris-buffered saline (TBS) for atomic force microscopy (AFM).”

3.7 Protein, lipid, and total phosphatidylcholine quantification of extracellular vesicles

To determine protein concentration of the EV isolates, light absorption at 280 nm was measured using an Implen N50 nanophotometer (Implen, München, Germany).

To measure total lipid content, the protocol of Visnovitz *et al*. [75] was used, that we briefly summarized earlier [71]:

“50 mg of vanillin (Sigma, W310727) was dissolved in 50 mL of 17% phosphoric acid (Sigma, 79617) to create phosphor-vanillin reagent. 200 µL of 96% sulfuric acid was either to 40 µL of 1,2-Dioleoyl-sn-glycero-3-phosphocoline (DOPC) (Sigma, P6354) liposome standards, or to 40 µL of EVs suspended in sterile filtered PBS. After being vortexed, samples and standards were incubated at 90 °C in a fume hood for 20 min. Tubes were cooled down and 120 µL of phospho-vanillin reagent was added to each tube, and 280 µL of each sample was transferred into a 96-well plate and was incubated at 37 °C for 1 h. Absorbance was determined at 540 nm using a plate reader (Multiskan Go, Thermo Scientific).”

To measure total phosphatidylcholine (PC) content of EV isolates, a colorimetric assay (CS0001, Merck KGaA, Darmstadt, Germany) was used according to the producer’s instructions.

3.8 Nanoparticle Tracking Analysis

Nanoparticle Tracking Analysis (NTA) was performed using a Zeta View PMX 110 device (Particle Metrix, Meerbusch, Germany). Measurements were performed as we described earlier [66]:

"The machine was calibrated using 100 nm polystyrene beads according to the manufacturer's protocol. Samples were diluted in PBS to have 50-300 particles in a view of sight. At least 1 mL sample was injected into the machine and automated measurement was acquired with 11 positions throughout the measurement cell, with two cycles of reading at each position. Readings for which the software recommended exclusion were excluded from the final evaluation."

Instrument parameters were set as: temperature 25 °C, sensitivity 75 for mEVs and 85 for sEVs, frame rate 7.5 frames per second for mEVs and 30 frames per second for sEVs, shutter speed 100. Post-acquisition parameters were set as: minimum brightness 20, minimum size 5 pixels, maximum size 1000 pixels. Results were multiplied by the dilution factor.

Results were analyzed using R programming language [74]. To visualize the size distribution of EVs, the mean of all measurements of each experimental groups was calculated, the data was smoothed with Loess-regression and visualized with ± SEM.

3.9 Atomic force microscopy imaging and force spectroscopy of small extracellular vesicles

Atomic Force Microscopy (AFM) of EV isolates was performed by the group of the Department of Biophysics and Radiation Biology, Semmelweis University. EV samples were 100-fold diluted in tris-buffered saline (TBS) solution, deposited on a freshly cleaved mica surface, and incubated at 25±1°C for 30 minutes. The surface was rinsed with ultrapure water and then kept in TBS. Samples were measured using a Cypher ES AFM (Asylum Research, Santa Barbara, CA) with Olympus BL AC 40 TS cantilevers (nominal stiffness: 90 pN/nm, resonance frequency: 110 kHz, tip radius: 8 nm; Olympus, Japan) at 2°C. Calibration was performed as described earlier [76]. Non-contact mode images were performed at a line scanning frequency of 0.5-1 Hz. Contact mode measurements were then performed for in situ force spectroscopy on spherical structures with height exceeding 15 nm. The cantilever was moved at a speed of 1 μm/s from a pre-

set height until a load threshold of 100 pN was reached, after which the cantilever was retracted with the same speed. Data were analyzed using the built-in software of the device (IgorPro, WaveMetrics Inc., Lake Oswego, OR). Structures with a minimal height of 10 nm were treated as EVs. EV diameter was defined as the diameter of a circle with an area equals to the surface area of the detected structure. Vesicle height was measured as the difference between the highest point of the vesicle and the substrate. Young's modulus was calculated by fitting force-vesicle indentation curves from 0 (contact point) to 100 pN loading force using the modified Hertz model [77].

3.10 Analysis of small extracellular vesicle proteomics

sEVs were isolated as described above, vacuum dried and transferred on dry ice to UCD Conway Institute Mass Spectrometry Resource where proteomics analysis was performed using liquid chromatography bound tandem mass spectrometry (LC-MS/MS). The samples were prepared as we described earlier [71]:

"Samples were then resuspended in 50 µL of 50 mM Tris HCl (Thermo Scientific, Waltham, MA, USA), sonicated, and protein concentration was measured using a bicinchoninic acid (BCA) assay kit (Thermo Scientific, Waltham, MA, USA). Samples were normalized to protein concentration and dissolved in 6 M Urea (Thermo Scientific, Waltham, MA, USA). The samples were then reduced by adding 8 mM of dithiothreitol (Merck KGaA, Darmstadt, Germany) and stirred at 30 °C at 1000 rpm for 30 minutes. Samples were then carboxylated by adding 20 mM of iodoacetamide (Merck KGaA, Darmstadt, Germany) and stirred at 30 °C at 1000 rpm for 30 minutes. Next, samples were diluted with 50mM of Tris HCL to reduce urea concentration below 2M. Samples were digested by Trypsin (Promega (Corporation, Madison, WI, USA) at 37 °C with 1000 rpm in 1:30 enzyme:sample ratio overnight. Digestion was terminated by adding formic acid (Thermo Scientific, Waltham, MA, USA) to 1% final concentration. Samples were purified on Empore™ Solid Phase Extraction membranes (Merck KGaA, Darmstadt, Germany), eluted in 60% acetonitrile and 0.1% Trifluoroacetic acid, vacuum dried and in 0.1% formic acid and each sample was loaded onto an Evosep tip (Evosep Biosystems, Buchwaldsgade, Denmark)."

LC-MS/MS measurements were performed by the UCD Conway Institute Mass Spectrometry Resource. Experiments were performed as we described earlier [71]:

"The Evosep tips were placed in position on the Evosep One, in a 96-tip box. The autosampler is configured to pick up each tip, elute and separate the peptides using a set chromatography method (30 samples a day)[ref.: [78]*]. The mass spectrometer was operated in positive ion mode with a capillary voltage of 1.700 V, dry gas flow of 3 l/min and a dry temperature of 180 °C. All data were acquired with the instrument operating in trapped ion mobility spectrometry (TIMS) mode. Trapped ions were selected for ms/ms using parallel accumulation serial fragmentation (PASEF). A scan range of (100-1700 m/z) was performed at a rate of 5 PASEF MS/MS frames to 1 MS scan with a cycle time of 1.03s[ref:* [79]*]. The following chromatography buffers were used: Buffer B: 99.9% acetonitrile, 0.1% formic acid. Buffer A: 99.9% water, 0.1% formic acid.*

LC-MS/MS data have been deposited to the ProteomeXchange Consortium via the PRIDE [80] partner repository with the dataset identifier PXD044594.

Raw data were processed by the UCD Conway Institute Mass Spectrometry Resource using the search engine Maxquant (release 2.1.4.0) [81]. Data were searched against the Homo sapiens subset of the Uniprot Swissprot database (reviewed, 12.11.2021) with specific parameters for trapped ion mobility spectra data dependent acquisition. Specific Maxquant parameters, i.e., only peptide scores that corresponded to a false discovery rate (FDR) of 0.01 were set to filter low quality data. Then, data were normalized using Label Free Quantitation (LFQ) [82].

We have analyzed LFQ intensities according to the protocol of Tyanova & Cox [83], using R programming language [74] as we described earlier [71]:

"Proteins that were labelled as 'reversed' or 'potential contaminants' or 'only identified by site' were excluded (see supplementary material). Proteins that were detected in less than half of the samples in all groups were also excluded. All other proteins were defined as identified and processed for quantitative analysis. Data were log2 transformed and the missing values were imputed with normal distribution around the detection limit."

Statistical analysis was applied on log2 transformed data, meanwhile, for fold-change calculation, non-transformed data was used. To visualize protein-protein interaction network and to perform gene ontology (GO) enrichment analysis STRING software [84,85] was used.

3.11 Culturing of THP1-ASC-GFP monocytes and treatment with AC16 sEVs

THP1 human monocytes expressing apoptosis-associated speck-like protein containing a CARD domain fused by green fluorescent protein (ASC-GFP, InvivoGen, Toulouse, France) were maintained as we described earlier [71]:

"[Cells] were maintained in THP1 medium consisting of RPMI 1640 medium (Gibco, 21875-034), 10 V/V% heat inactivated FBS (Corning, 35-079-CV), 1% L-glutamine (Corning, 30-004-CI), 1 % antibiotics-antimycotics (Corning, 25-005-CI), and 1% HEPES (Gibco, 15630-080) at a maximum of 6×10^5 cells/mL in a T175 flask. THP1 medium was also supplemented with 100µg/mL Zeocin (InvivoGen, ant-zn-0.5) for transgene selection at every second passage. Cells were grown at 5% CO2 95% air, at 37°C."

For monocyte activation assay, 1×10^6 THP1-ASC-GFP cells were treated with a final concentration of 10^7, 10^8 or 10^9 particles/mL AC16 sEVs or with 100 ng/mL lipopolysaccharides in one mL culturing medium for 16 hours.

3.12 Flow cytometry of THP1-ASC-GFP monocytes

THP1-ASC-GFP cells were treated with AC16 sEVs as described above. Cells were then centrifuged, resuspended in PBS, and fixed with 1% PFA at 4 °C for 10 min followed by two washes with PBS. Flow cytometry was performed by Szabolcs Hambalkó (Semmelweis University, Department of Pharmacology and Pharmacotherapy) using BD FACSCalibur (BD Biosciences, San Jose, CA, USA). Forward and Side scatter and GFP expression were analyzed using Flowing software (Turku Bioscience, Turku, Finland) to select viable cells and to measure the percentage of the GFP^+ population. For each measurement, 10,000 events were counted.

3.13 Quantitative PCR of THP1-ASC-GFP monocytes

THP1-ASC-GFP cells were treated with AC16 sEVs as described above. The cells were then lysed in Qiazol lysis reagent (Qiagen, Germantown, MD, USA) and stored at -80 °C. To isolate RNA, samples were centrifuged at 4 °C at 12,000 × g for 10 minutes. Supernatants were then mixed with chloroform (Thermo Scientific, Waltham, USA) in 5:1 ratio, incubated for 3 minutes at room temperature and centrifuged at 4 °C at 120,000

× g for 15 minutes. Supernatant was collected and mixed with isopropanol (Merck KGaA, Burlington, USA) in 1:1 ratio and centrifuged at 4 °C with 12,000 × g for 10 minutes. The supernatant was removed, pellet was washed with 75% ethanol (VWR, Randor, PA, USA) and centrifuged at 4 °C at 12,000 × g for 10 minutes. The pellets were dried and resuspended in RNase-free water. SensiFAST cDNA synthesis kit (Bioline; London, UK) was used to prepare cDNA according to the manufacturer's protocol. PCR measurements were performed on a LightCycler® 480 Real-Time PCR System (Roche Diagnostics, Basel, Switzerland) using LightCycler® RNA Master SYBR Green I reagent (Roche Diagnostics, Basel, Switzerland) with primers presented in Table 1. The PCR protocol was set as: Initiation: 95 °C for 2 min; Amplification: 45 cycles of 95 °C for 5 s, then 57 °C for 10 s, then 72 °C for 20 s; final extension: 7 2°C for 5 min. Data were analyzed using the ΔΔCt calculation method according to Schmittgen and Livak 2008 [86]. Hypoxanthine Phosphoribosyltransferase 1 was used as the housekeeping gene.

Table 1.: PCR primers used for gene expression analysis of THP1-ASC-GFP monocytes after treatment with AC16 sEVs.

Gene name	Gene abbreviation	Primers sequence
Interleukin 1 Beta	IL-1b	5′-ATTGCTCAAGTGTCTGAAGCAGC-3′ 5′-AGCCCTTGCTGTAGTGGTGG-3′
Interleukin 10	IL-10	5′-GCCTTCAGCAGAGTGAAGACTTTCTTTC-3′ 5′-CCAGGTAAAACTGGATCATCTCAGACAAGGC-3′
Hypoxanthine Phosphoribosyltransferase 1	HPRT	5′-TGCTCGAGATGTGATGAAGG-3′ 5′-TCCCCTGTTGACTGGTCATT-3′
Tumor Necrosis Factor-Alpha	TNF-α	5′-ATACTGACCCACGGCTCCAC-3′ 5′-AGAAGATGATCTGACTGCCTGGG-3′
Interleukin 6	IL-6	5′-GGTACATCCTCGACGGCATCT-3′ 5′-GTGCCTCTTTGCTGCTTTCAC-3′

3.14 Isolation and culturing of neonatal rat cardiac fibroblasts

Neonatal rat cardiac fibroblasts (NRCF) were isolated from 1-3 day-old male Wistar rats (Toxi-coop ltd., Budapest, Hungary) according to the protocol optimized by Marek Jelemenský [66]. Animals were sacrificed by cervical dislocation, the hearts were removed and placed into cold PBS. Then, atria were removed, and the tissue was minced and digested in 0.25% trypsin solution (Thermo Scientific, Waltham, MA) at 37 °C for 25 minutes with agitation in every 5 minutes. The resulting cell suspension was

centrifuged for 15 minutes at 250 rcf at 4 °C. The supernatant was removed, and the pelleted cells were resuspended in Dulbecco's Modified Eagle Medium (Corning Inc., NY, USA) supplemented with 10% FBS (Corning Inc., NY, USA) and seeded into a cell culture flask. After 90 minutes, the culturing medium was collected and transferred into a fresh culture flask to seed NRCFs. Cells were subcultured when 75% of confluence was reached using 0.5% trypsin/0.53 mM EDTA (ATCC, Manassas, VA, USA). Cells were used for no longer than three passages.

3.15 Helium conditioning of neonatal rat cardiac fibroblasts

NRCFs at 75-90% of confluence in cell culture flasks were employed for HeC according to the protocol optimized by Marek Jelemenský [66]. Cells were washed with Hanks balanced salt solution (HBSS, Corning Inc., NY, USA) and then glucose- and FBS-free growth medium (PAN-Biotech GmbH, Aidenbach, Germany) was added. The flasks were placed into a sealed plastic container with loosened caps. To ensure removal of all room air, the container was filled and flushed with 95% helium + 5% CO_2 gas mixture four times, then fully filled with the gas mixture, and sealed. Flasks were incubated at 37°C for 1 hour in the hermetic container. After incubation, the container was opened and the flasks were left under normal growth conditions (5% CO_2 /95% air, 37°C) for 1 hour. This treatment was repeated a total of four times. After the fourth cycle of treatment, culturing medium was supplemented with 1g/L glucose (Merck KGaA, Burlington, USA) and the flasks were left in normal growth conditions for 40 hours. For control, cells were kept under normal growth conditions in the same culturing medium that the HeC-treated cells. When NRCF supernatant was used for HUVEC-TERT2 angiogenesis or migration assay, the media used for conditioning were replaced with FBS- and bovine brain extract (BBE)-free HUVEC-TERT2 growth medium.

3.16 Electron microscopy of extracellular vesicles

For transmission electron microscopy (TEM), mEVs were resuspended in 1.5 mL PBS and centrifuged for 1 hour at 100,000 rcf at 4 °C in a polypropylene ultracentrifuge tube. Samples were fixed within the tube with 4% paraformaldehyde and then with 1% osmium tetroxide (Taab, Aldermaston, UK). Samples were dehydrated in graded ethanol, block-stained with 1% uranyl acetate in 50% ethanol, and embedded in Taab 812 (Taab,

Aldermaston, UK). After overnight incubation at 60 °C, pellets were sectioned using a Leica UCT6 ultramicrotome (Leica Microsystems, Wetzlar, Germany, UK). Images were taken with a Hitachi 7100 transmission electron microscope (Hitachi Ltd., Tokio, Japan) and a Veleta 2 k × 2 k MegaPixel side-mounted TEM CCD camera (Olympus, Tokio, Japan). Brightness and contrast were adjusted using Adobe Photoshop 7.0 (Adobe Systems Incorporated, San Jose, CA, USA).

3.17 Culturing of HUVEC-TERT2 cells

HUVEC-TERT2 endothelial cells were cultured as we described earlier [66]:

"HUVEC-TERT2 (Evercyte GmbH, Vienna, Austria, CHT-006-0008) were cultured on 0.1% gelatin (Merck KGaA, Burlington, USA)-coated surface using endothelial cell growth basal medium (Lonza Group Ltd, Basel, Switzerland), supplemented with human endothelial growth factor, hydrocortisone, bovine brain extract (BBE), ascorbic acid and FBS from Lonza SingleQuots Kit (Lonza Group Ltd, Basel, Switzerland) and 20 µg/mL G418 solution (Roche Diagnostics, Basel, Switzerland). Cells were kept at 37°C in 5% CO_2/95% air environment and subcultivated according to the vendor's protocol, when cells reached 80% of confluence."

3.18 HUVEC-TERT2 migration assay

In vitro migration assay of HUVEC-TERT2 cells were performed as we described [66]:

"HUVEC-TERT2 were seeded onto 24-well plate and grown until confluence. Sixteen hours before the assay, medium was changed to growth medium supplemented with 1% FBS and 0.25% BBE. After incubation, confluent cell monolayer was scratched off from the surface using a 1000 µL pipette tip and growth medium from HeC NRCF or CTRL NRCF supplemented with 1% FBS and 0.25% BBE was added onto the cells. Pictures from each well were taken in two defined positions at 0 hours and 8 hours using phase contrast microscope (Leica Microsystems, Wetzlar, Germany). Images were analyzed using ImageJ software by a blinded analyzer. For each image, area of the scratch was measured, and percentage of the gap closure was calculated. At each experiment, images from the same well were analyzed individually and then the average of the gap closure values was calculated and treated as a single data point."

3.19 Tube formation assay of HUVEC-TERT2 cells

For HUVEC-TERT2 tube formation assay, culture media of HeC-treated or control NRCFs were collected and supplemented with 5% FBS and 0.25% BBE. HUVEC-TERT2 cells were then subcultured at a seeding density of 8000 cells/well using the collected media in Ibidi angiogenesis µ-slides (Ibidi GmbH, Gräfelfing, Germany) coated with Matrigel basement membrane (Corning Inc., New York, USA). Images were taken 6 hours after incubation using a phase contrast microscope (Leica Microsystems, Wetzlar, Germany, UK). Image analysis was performed using the ImageJ [87] Angiogenesis Analyzer macro [88]. Each individual data points represents the average of three technical replicates. *Number of master junctions* represents the number of nodes, *mean mesh size* represents the mean size of the meshes and *Mesh index* represents mean tube length.

3.20 sodium dodecyl sulfate polyacrylamide gel electrophoresis and western blotting

For western blot analysis, samples were lysed in 10x radio-immunoprecipitation assay buffer (RIPA; Cell Signaling Technology, Danvers, MA, US) containing protease inhibitor (Amresco, Solon, OH, US) at a sample-to-buffer ratio of 1:10. Equal volume of samples were then mixed with 1/4 volume of Laemmli buffer containing β-mercaptoethanol (Thermo Scientific, Waltham, MA, USA) and incubated at 96°C for 5 minutes. Samples were loaded onto Tris-glycine sodium dodecyl sulfate-polyacrylamide gels (Bio-Rad, Hercules, CA, USA) and gel electrophoresis was performed using Criterion Cell and PowerPac Basic Power Supply (Bio-Rad, Hercules, CA, USA). Proteins were then transferred to polyvinylidene difluoride membranes (Bio-Rad, Hercules, CA, USA) and blocked with 5% bovine serum albumin (Bio-Rad, Hercules, CA, USA) in TBS containing 0.05% Tween-20 at room temperature for 2 h. Primary antibodies used are detailed in Table 2. As secondary antibodies, Anti-mouse IgG, HRP-linked Antibody (7076s, Cell Signaling Technologies, Danvers, MA, USA) and Anti-rabbit IgG, HRP-linked Antibody (7074s, Cell Signaling Technologies, Danvers, MA, USA) were used. Signals were visualized using ECL chemiluminescence kit (Bio-Rad, Hercules, CA, USA) and Chemidoc XRS+ (Bio-Rad, Hercules, CA, USA). Data analysis was performed using Image Lab software (Bio-Rad, Hercules, CA, USA) was used.

Table 2.: Antibodies used in Western Blot analyses.

Target name	Target abbreviation	ID	Vendor
Albumin	Albumin	sc-271605	Santa Cruz Biotechnology
Annexin A1	ANXA1	ab214486	Abcam
Apolipoprotein B-100	ApoB	MABS2046	Merck
ATP synthase subunit alpha	ATP5A	ab133989	Abcam
CD81 antigen	CD81	sc-166029	Santa Cruz Biotechnology
Fibrinogen beta chain	FGB	GTX54019	GeneTex
Glyceraldehyde-3-phosphate dehydrogenase	GAPDH	ab133989	Abcam
Heat shock 70 kDa protein	HSP70	sc-66049	Santa Cruz Biotechnology
Histone-H3	Histone-H3	ab133989	Abcam
Programmed cell death 6-interacting protein	ALIX	sc-53540	Santa Cruz Biotechnology
Sodium Potassium ATPase	Na-K-ATPase	ab133989	Abcam
Tumor susceptibility gene 101 protein	TSG101	ab83	Abcam

3.21 Statistics and visualization

Statistical data analysis and data visualization were implemented using R programming language [74] with ggplot2 package [89] and GraphPad Prism 6 software (GraphPad Software Inc., San Diego, CA, USA). Adobe illustrator (Adobe, San Jose, CA, USA) was used to create figures. All figures are the original work of the author, or the reference is highlighted in the figure legend. All referenced figures are freely re-usable according to the Creative Commons Attribution 4.0 International License CC-BY license.

To compare metabolome of NC and HC rat plasma and pEVs, multiple t-tests with Benjamini-Hochberg FDR adjustment were applied, while linear regression analysis was used for the correlation of plasma and pEV metabolome. To analyze AC16-derived sEVs, including particle size and concentration measurement with NTA, protein concentration measurement, particle size, concentration and elasticity measurement with AFM, total lipid measurement, relative PC concentration measurement, the analysis of lipid-to-

protein ratio and for the analysis of the results obtained from the treatment of THP1-ASC-GFP cells with AC16 sEVs, analysis of variance (ANOVA) with Tukey's post-hoc test was applied. For the quantitative analysis of AC16 sEV proteomics, ANOVA with FDR adjustment followed by Tukey's post-hoc test was used, For GO analysis, enrichment analysis with FDR correction was applied using the STRING software [84,85]. For the statistical analysis of NRCF mEV secretion and HUVEC-TERT2 treatment with NRCF mEVs, Wilcoxon t-test was used. Data are presented as mean ± standard error of the mean. Significance level was set as $\alpha = 0.05$.

4 Results

4.1 Hypercholesterolemia dysregulates plasma-derived extracellular vesicle metabolome independently of plasma metabolome

Discovering of how metabolic diseases dysregulate pEVs can augment our understanding of the pathomechanism of these disorders. Numerous studies have demonstrated that the number of pEVs increases in metabolic disorders [41–43]. Furthermore, the protein and miRNA composition of pEVs in obesity have also been addressed [48,50]. To further understand how metabolic diseases, especially HC, affects pEVs, we investigated how HC diet modifies the metabolite composition of pEVs in rats and how this correlate with the plasma metabolome (Figure 1A). We fed rats with hypercholesterolemic chow for twelve weeks, then we collected plasma samples and isolated pEVs using density gradient ultracentrifugation followed by size exclusion chromatography with a protocol results in EV isolates with non-detectable amounts of common contaminants, such as Apolipoprotein A1, as we have shown earlier [73].

Using a commercial kit we have analyzed the presence of 630 pre-defined metabolites, out of which 433 were detected in plasma and only 29 in pEVs [71]. To test our animal model system, first we analyzed metabolite composition of the plasma samples. We have identified a significant increase in the aggregated intensities of cholesterol esters upon the treatment (Figure 1C). Furthermore, several triacylglycerols showed increased concentration, whereas multiple glycerophospholipids had decreased concentration (Figure 1D, left panel). Despite these changes the body weight of the animals remained unchanged (Figure 1B). These results indicate that our animal model system represents non-obese patients with HC well.

Next, we have analyzed the pEV metabolome, to unravel how HC dysregulates the metabolite composition of EVs in the circulation. We identified that EVs from HC-fed rat contained significantly less amount of several PCs (Figure 1D, right panel). When we compared these data with metabolite intensities obtained from plasma samples, we identified that some of these PCs showed opposite changes (Figure 1E). To further analyze the connection between plasma and pEV metabolites, we correlated intensities of metabolites detected in both plasma and in pEVs from the same animal. Surprisingly, there was no correlation between plasma and pEVs in the concentration of amino acids,

amino acid-related metabolites, fatty acids, and triacylglycerols, and only a moderate correlation was identified in the concentration of glycerophospholipids (Figure 1F). This analysis highlights that HC dysregulates not only plasma metabolome, but also pEV metabolite composition. Furthermore, these changes are differentially regulated. These results indicate that pEVs might have a different biological effect in HC, and novel pathomechanism can be discovered with their analysis, which were hidden if plasma was measured alone.

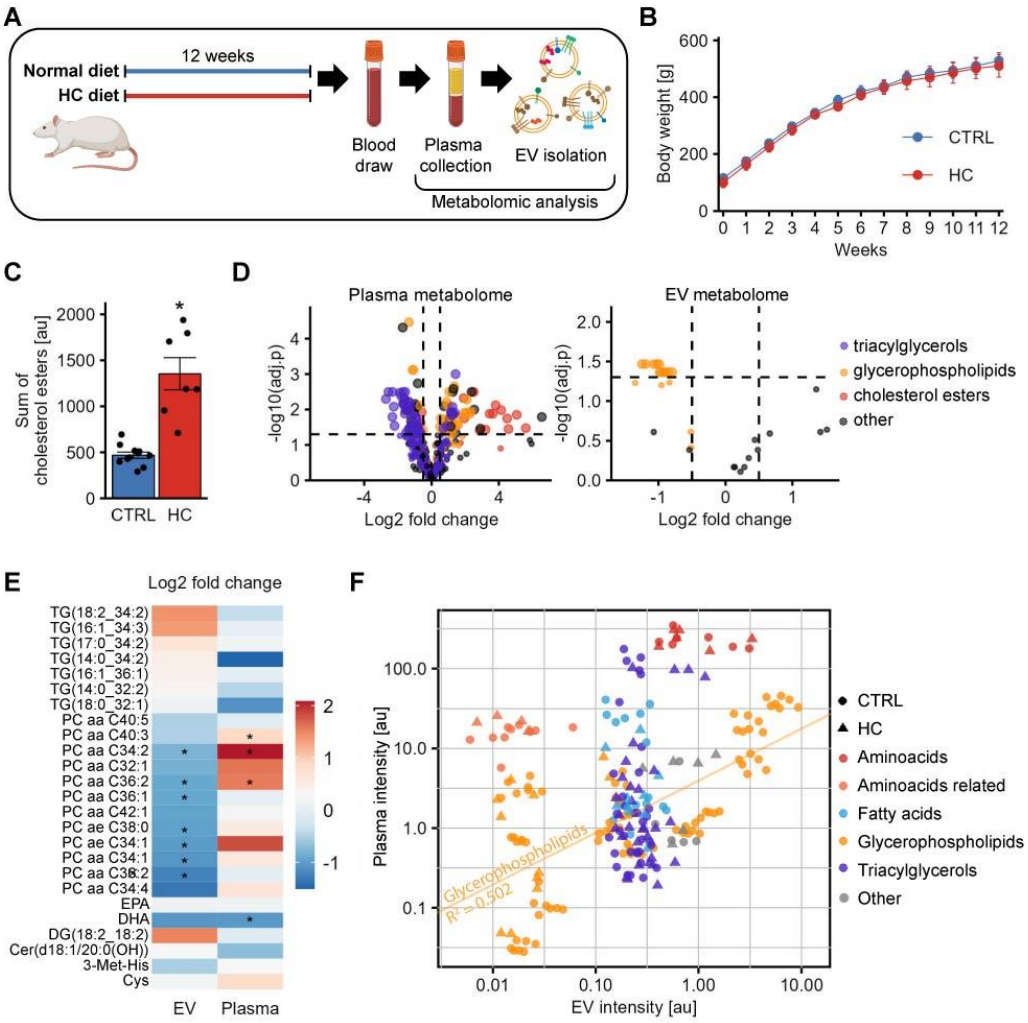

Figure 1.: Effect of hypercholesterolemia on circulating extracellular vesicle metabolome. *(A) Schematic representation of the experimental plans. Male Wistar Rats were fed either with normal or HC chow for twelve weeks, when serum samples were collected and serum EVs were isolated. Metabolomics of both sample types were measured. (B) Animal body weight was unaffected by the treatment. (C) Aggregated intensity of cholesterol esters was significantly enriched by HC treatment. (D) Volcano plots representing the differentially regulated metabolites in (left panel) plasm and in (right panel) EVs.* *[Figure legend continues on page 27.]*

Figure 1. continued: Effect of hypercholesterolemia on circulating extracellular vesicle metabolome *(E) Comparison of fold changes in those metabolites that were statistically analyzed both in plasma and EVs. Opposite direction of changes was observed at certain phosphatidylcholines. (F) Linear correlation in the metabolite groups analyzed between plasma and EVs. Each dot represents a single metabolite measured in both samples. Correlation was observed in the amount of glycerophospholipids only, with* $R^2 = 0.502$. * $p < 0.05$ *between CTRL and HC groups in Student's t-test. HC: Hypercholesterolemia, CTRL: Normal-fed group, EV: Extracellular vesicle. Obtained from Kovácsházi et. al* [71].

4.2 Hypercholesterolemia increases cardiomyocyte extracellular vesicle secretion without changing its phosphatidylcholine concentration

Cardiovascular derangements by HC through EVs can originate from both circulating pEVs and EVs secreted in the local microenvironment. As CMs are the major functioning elements of the myocardium, we focused our research on understanding how HC dysregulates CM EV secretion to identify potential pathological effects driven by EVs.

We have treated AC16 human CMs with hypercholesterolemic supplement or with its vehicle and isolated sEVs using differential centrifugation (Figure 2A). To validate our HC treatment, we stained accumulated lipids in AC16 cells with Oil-red-O stain. We confirmed that the lipid content was increased due to HC treatment (Figure 2B).

Next, we have analyzed the protein content of our sEV isolate using Western Blotting to test the purity of our isolates according to the guidelines [25]. We detected EV markers tumor susceptibility gene 101 and programmed cell death 6-interacting protein, and transmembrane EV protein CD81 in our samples. Additionally, we detected glyceraldehyde-3-phosphate dehydrogenase (GAPDH) and heat shock protein 70, which are common cargo proteins of EVs. We tested for potential contaminants by measuring ATP synthase lipid-binding protein (ATP5A), sodium potassium ATPase (Na-K-ATPase) and Histone H3, out of which the samples were positive for Histone H3 (Figure 2C). These results suggest that EVs were enriched in our isolate and most of common EV contaminants, such as fragments of membrane-bound organelles were below the detection limit.

We used NTA to determine the EV size and concentration of our isolates. We identified particles between 50-300 nm (Figure 2D) with a median size of 150 nm, regardless of the treatment (Figure 2E). These results demonstrate that we successfully isolated small-sized EVs.

NTA data analysis also revealed that HC treatment significantly elevated particle level in HC-treated AC16 sEV isolates (Figure 2F). Similarly, we found that the protein concentration of these samples was also increased (Figure 2G). These results suggest that HC increases CM sEV secretion, aligning with the systemic effect of HC, as pEV concentration is also increased in certain metabolic diseases [41–45].

As we observed a decreased amount of certain PCs in rat pEVs, we proceeded to analyze the lipid-to-protein ratio and relative PC concentration of AC16 sEV isolates. However, our analysis did not reveal difference in the lipid-to-protein ratio of the samples (Figure 2H). Similarly, the PC concentration, normalized to the total lipid concentration of AC16 sEVs, was unaffected by HC treatment (Figure 2I).

To further analyze the membrane composition of AC16 sEVs in HC we conducted AFM measurements on our sEV isolates with the Department of Biophysics and Radiation Biology of Semmelweis University. As cholesterol affects rigidity, banding and elasticity of plasma membranes [90–92], we hypothesized that HC treatment might modify the elasticity of EVs via increased cholesterol content of the membrane or other metabolic dysregulation. We observed that elastic moduli of sEVs distributed between 10^5-10^7 Pa (Figure 2J), which is consistent with earlier data on liposomes and EVs [93–95]. However, the treatment did not affect the elasticity of AC16 sEVs (Figure 2J). These results suggests that unlike in pEVs, the membrane composition of CM sEVs is not affected by HC or such changes were undetectable with our measurement system.

To verify our sEV isolation protocol, we analyzed our AFM data further. Surface mapping of AC16 sEVs revealed roughly circular particles with partially flattened, curved surfaces, that aligned with the literature [93,96–98]. Besides EVs, we identified smaller, rounded, or multisegmented objects with a height lower than 10 nm, likely lipid- or protein aggregates or vesicle fragments (Figure 2H). EVs ranged from 10 to 300 nm in diameter with a median size of around 50 nm (Figure 2L) and heights ranging from 10 to 100 nm (Figure 2M). As NTA cannot detect particles below 50nm, and overestimates particle size [99], these results align with our earlier measurements. Surprisingly, we found statistically significant difference in size between VEH vs CTRL or HC groups (Figure 2L) and in height between HC vs CTRL or VEH groups (Figure 2M), likely due to the high power of our measurements and as the effect size is minimal, the biological significance of these changes is probably negligible. Altogether, our observations validate

that we isolated sEVs from AC16 cells with minor contamination with non-vesicular fragments.

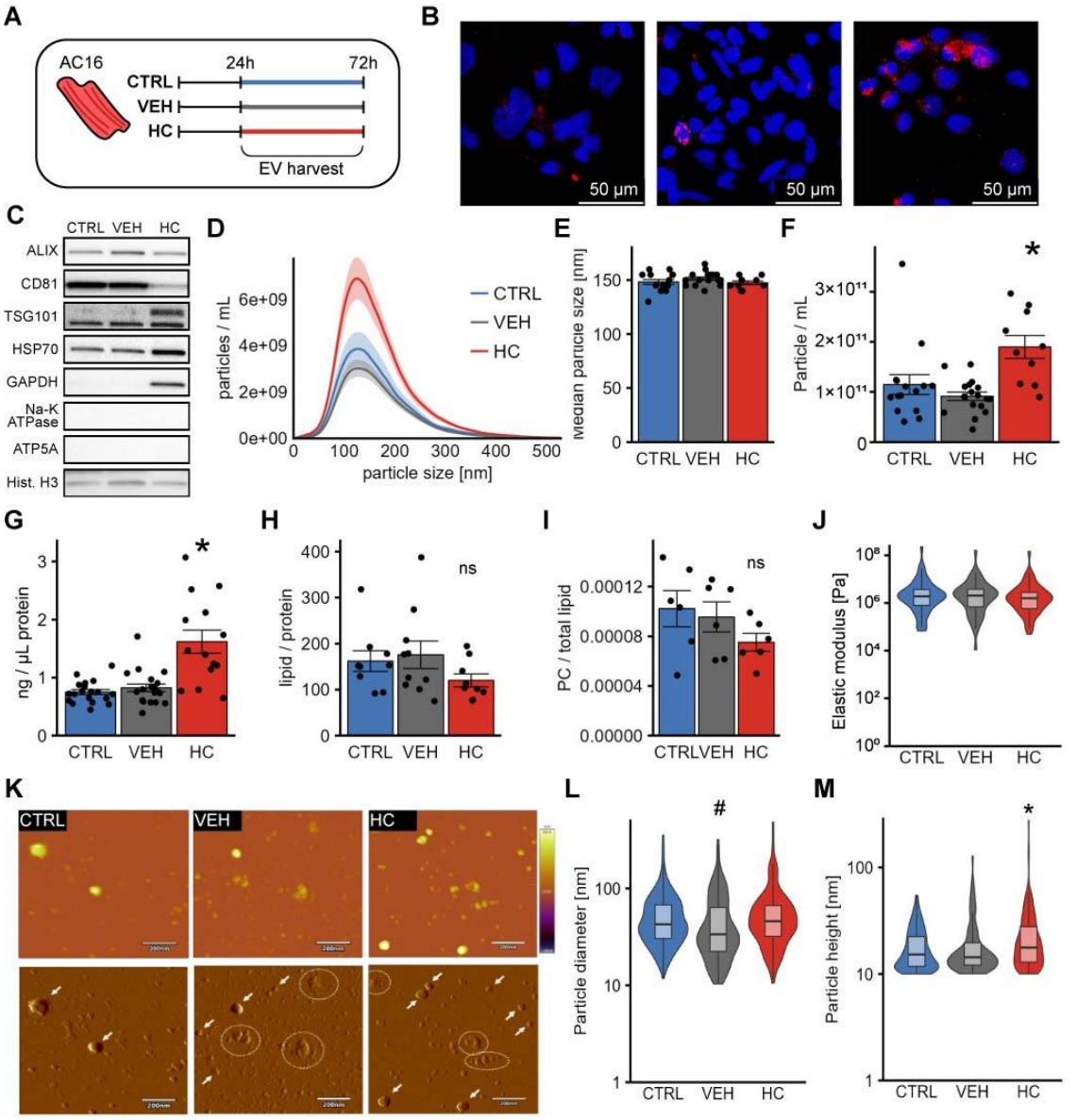

Figure 2.: Analysis of AC16 cardiomyocyte extracellular vesicles in hypercholesterolemia. *(A) Schematic representation of the experimental plans. AC16 cardiomyocytes were treated with HC treatment or with its vehicle or kept in control conditions and then EVs were isolated from the cell culture supernatant. (B) Representative images of Oil-red-o staining of AC16 cell after treatment. Blue: DAPI (nuclei), red: Oil-red-O (lipid). Results show increased amounts of lipids upon the treatment. (C) Western blot analysis on the EV isolates. Samples were free from most common contaminants and positive for extracellular vesicle markers. (D) Size distribution of isolated EVs measured by nanoparticle tracking analysis. Vesicles ranged from 50-300 nm (E) Median size of the detected particles. The treatment did not affect particle size (F) Particle number of the isolates was significantly elevated in HC group. (G) Protein concentration measured with 280 nm light absorbance was significantly elevated in HC group.* *[Figure legend continues on page 30.]*

Figure 2. continued: Analysis of AC16 cardiomyocyte extracellular vesicles in hypercholesterolemia. *(H) Lipid-to-protein ratio of EV isolates were unaffected by the treatment. (I) PC concentration normalized to total lipid concentration of EVs was unaffected by the treatment. (J) Elastic modulus of EVs analyzed with atomic force microscopy did not change upon the treatment. (K) Representative images of non-contact mode atomic force microscopy measurements. First row: height-contrast, second row: amplitude-contrast images in the same view field. Arrows: EVs, Circles: Non-EV-like structures with height < 10 nm. (L) In particle diameter measured by atomic force microscopy, a significant difference was observed between the VEH vs CTRL and HC groups. (M) In particle height measured by atomic force microscopy, a significant difference was observed between the HC vs CTRL and VEH groups. * p < 0.05 HC vs CTRL and VEH, # p < 0.05 VEH vs CTRL and HC in ANOVA with Tukey's post-hoc test. CTRL: Control conditions, VEH: Vehicle treatment, HC: Hypercholesterolemic treatment, ALIX: ALG-2-interacting protein X, TSG101: Tumor susceptibility gene 101, HSP70: heat shock protein 70, GAPDH: glyceraldehyde-3-phosphate dehydrogenase, Na-K-ATPase: Sodium-potassium ATPase, ATP5A: ATP synthase lipid-binding protein, Hist. H3: Histone H3, PC: phosphatidylcholine. Obtained from Kovácsházi et. al* [71].

4.3 Hypercholesterolemia do not modify the effect of cardiomyocyte extracellular vesicles on immune cells

One of the mechanisms contributing to HC-induced CVDs is inflammation. As EVs play a role in mediating inflammation through various mechanisms [24], we hypothesized that HC might alter the impact of CM-derived EVs on immune cells, as observed in other diseased conditions [53–56]. To test this hypothesis, we treated THP1 monocytes expressing ASC-GFP with sEVs derived from AC16 CMs at different doses. Following a 16-hour treatment. We measured GFP expression of monocytes with flow cytometry representing ASC expression that demonstrates inflammasome activation [100]. In addition, we analyzed the gene expression of certain cytokines to further investigate potentially activated pro- and anti-inflammatory signaling pathways (Figure 3A).

Our results showed that sEVs did not increase GFP expression in THP1-ASC-GFP cells regardless of the treatment applied to the donor cells (Figure 3B). This indicates that CM-derived sEVs do not trigger inflammasome activation in monocytes. To explore other, non-ASC dependent inflammasome-mediated mechanisms, we measured the gene expression levels of pro-inflammatory factors Interleukin 1 beta and Tumor Necrosis Factor alpha, as well as the anti-inflammatory factor Interleukin 10. No significant changes were observed in the expression of these genes, irrespective of the treatment (Figure 3C). These findings suggest that, contrary to our initial hypothesis, CM-derived sEVs do not contribute to inflammation in HC.

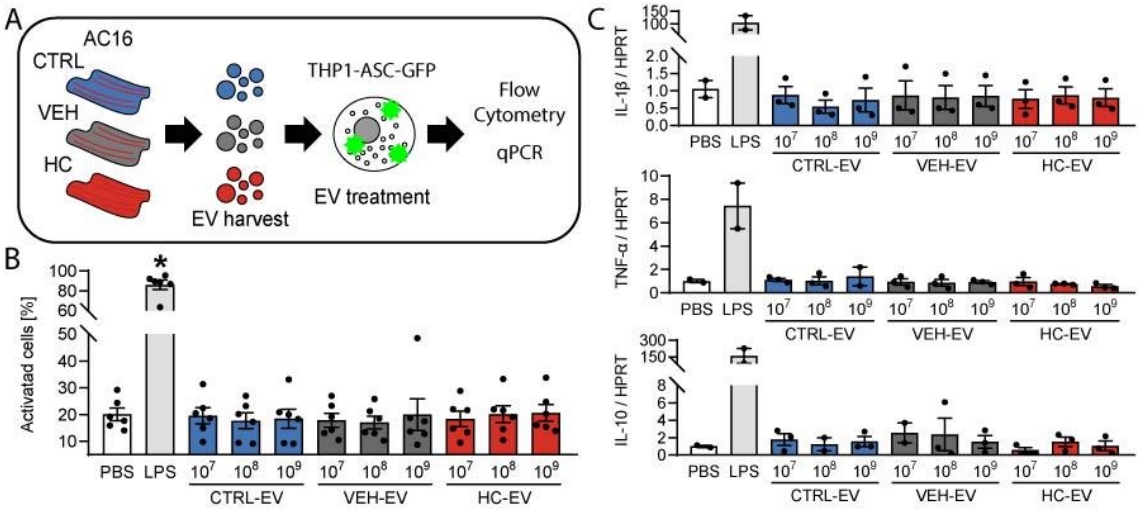

Figure 3.: THP1-ASC-GFP treated with AC16 extracellular vesicles. *(A) Schematic representation of the experimental plans. THP1-ASC-GFP monocytes were treated with EVs isolated from AC16 cells after HC treatment. GFP and gene expression of the monocytes were measured. (B) GFP expression of THP1-ASC-GFP cells after EV treatment. No difference was observed in the amount of GFP positive/activated cells. (C) The treatment did not affect the gene expression IL-1β, TNF-α and IL-10 genes. * $p < 0.05$ vs PBS in ANOVA with Tukey's post-hoc test. CTRL: Control conditions, VEH: Vehicle treatment, HC: Hypercholesterolemic treatment, EV: extracellular vesicle, IL-1β: Interleukin 1 beta, TNF-α: Tumor Necrosis Factor alpha, IL-10: Interleukin 10. Obtained from Kovácsházi et. al* [71].

4.4 Hypercholesterolemia dysregulates proteome of cardiomyocyte-derived extracellular vesicles

Contrary to our hypothesis, HC does not seem to modify the inflammatory effect of CM sEVs. In light of these results, we decided to analyze the protein composition of AC16 sEVs to identify potential functional dysregulations induced by HC.

Isolated AC16 sEVs were vacuum dried and transferred to the UCD Conway Institute Mass Spectrometry Resource for proteomics measurements using LC-MS/MS.

From all the samples measured, we identified a total of 2235 proteins derived from 2218 genes (available at the online supplementary material of the original article [71]). To perform a first quality control on our dataset, we compared these genes with the Vesiclepedia [101,102] database, which compiles thousands of proteomics studies on EVs. A total of 2088 genes overlapped with the database, including 84 of the 100 most frequently identified proteins in EVs (Figure 4A). These results highlight that nearly all identified proteins presented in at least one independent EV-proteomics study, and our sEV isolate show no major differences from others at the protein level.

To assess the effect of HC on the CM sEV proteome, we compared the protein abundance between our treatment groups using ANOVA with FDR adjustment and Tukey's post-hoc test. A total of 117 proteins showed statistically significant differences between at least one comparison. Of these, 12 proteins showed differences between the CTRL and VEH groups. Five of these 12 proteins had significantly different abundance between the CTRL and HC groups, but not between the VEH and HC groups. In addition, two proteins showed significant difference between the CTRL and HC groups, but not between the VEH and HC groups. A total of 110 proteins exhibited significant differences between the VEH and HC groups; all of these also showed significant differences between CTRL and HC groups (Table 3, Figure 4B). We selected these proteins for further analysis to explore proteomic changes induced by HC treatment in CM-derived sEVs.

Among the 110 proteins analyzed, the abundance of 33 proteins decreased in sEVs derived from HC-treated AC16 cells (Figure 4C). These included numerous extracellular matrix (GO: 0031012, FDR < 0.001) and cell adhesion-associated (GO: 0005925, FDR < 0.001) proteins. Additionally, the amount of certain endosomal sorting complexes required for transport (ESCRT) constituents [103] was reduced (Figure 4D, left panel).

Most of the 77 proteins with increased abundance in HC-treated AC16 sEVs were associated with RNA binding (GO:0003723, FDR < 0.001). Some of these, such as nuclease-sensitive element-binding protein 1, heterogeneous nuclear ribonucleoproteins A2/B1 and heterogeneous nuclear ribonucleoprotein A1 (HNRNPA1) [104–109], are involved in RNA packaging into EVs as well. Additionally, many of these proteins are part of the spliceosome or ribosomal complex (Figure 4D, right panel). This suggest that not only the protein but also the RNA composition of CM EVs are affected by HC.

We further investigated the functions of the dysregulated proteins, which might play a role in HC-induced CVDs. Numerous proteins with increased abundance in HC-treated AC16 sEVs are associated with tissue remodeling, namely connective tissue growth factor, also known as cellular communication network factor 2, which mediates fibrosis in cardiomyocytes and regulates proliferation, cell adhesion and angiogenesis [110], as well as cysteine-rich angiogenic inducer 61, also known as cellular communication network factor 1 (CYR61, CCN1), DNA (cytosine-5)-methyltransferase 1 (DNMT1) and HNRNPA1 which play a role in EV-induced angiogenesis, proliferation, invasion or in

vivo metastasis formation of cancer EVs [111–113]. Furthermore, CYR61 encapsulated in EVs also induces Metalloproteinase 1 expression in recipient cells [114].

Additionally, proteins such as DNMT1, HNRNPA1, Double-stranded RNA-binding protein Staufen homolog 1 and Gamma-interferon-inducible protein 16, which had increased abundance in HC-treated AC16 sEVs, regulate genes involved in lipid metabolism and adipocyte differentiation [115–118].

Finally, none of the proteins enriched in AC16 sEVs after HC treatment were associated with inflammation. On the contrary, the immunogenic protein HLA class I histocompatibility antigen, B-7 alpha chain decreased in abundance in sEVs of the HC group.

In conclusion, proteomics analysis of AC16 sEVs revealed that HC substantially modifies CM EV proteome and potentially affects EV RNA content as well, that can modulate the biological function of EVs.

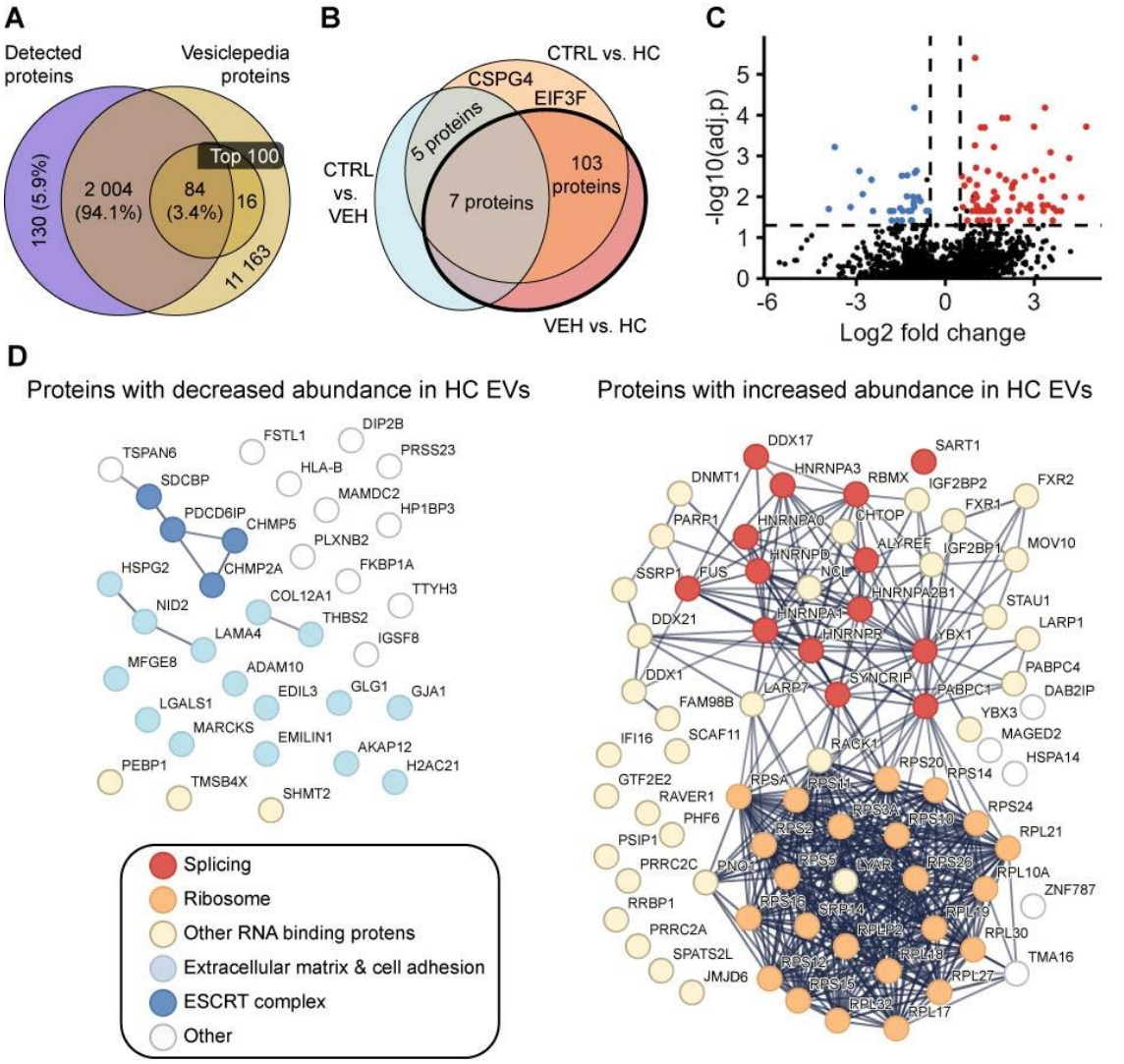

Figure 4.: Proteomic analysis of AC16 extracellular vesicles. *(A) Comparison of the proteins detected with the Vesiclepedia database. Out of the 2137 proteins identified, 2088 are part of the database of which 84 are in the 100 most frequently described EV proteins. (B) Venn diagram representing the statistically significant differences between the experimental groups, using ANOVA followed by Tukey's post-hoc test. (C) Volcano plot representing the significant differences between the VEH and HC groups. (D) Interaction network of proteins with significantly different abundance between the VEH and HC groups. LEFT: Proteins with decreased abundance, RIGHT: Proteins with increased abundance. CTRL: Control conditions, VEH: Vehicle treatment, HC: Hypercholesterolemic treatment, EV: extracellular vesicle, ESCRT: endosomal sorting* complexes *required for transport. Obtained from Kovácsházi et. al* [71].

Table 3.: List of proteins found differentially expressed in AC16 small extracellular vesicles upon hypercholesterolemic treatment. *Proteins found significantly different between VEH and HC groups were involved in further analysis. * $p < 0.05$ for ANOVA followed by Tukey's post-hoc test. Obtained from Kovácsházi et. al* [71].

#	Protein IDs	Gene names	ANOVA post-hoc significance			Log2 fold change		
			CTRL vs VEH	CTRL vs HC	VEH vs HC	CTRL vs VEH	CTRL vs HC	VEH vs HC
1	O14672;O14672-2	ADAM10	*	ns	*	-0.323	-1.762	-1.439
2	P25098;P35626	ADRBK1;ADRBK2	*	*	ns	3.492	4.442	0.950
3	Q02952-3;Q02952-2;Q02952	AKAP12	*	ns	*	-0.163	-1.324	-1.161
4	Q86V81	ALYREF	*	*	*	1.878	4.210	2.332
5	O43633	CHMP2A	*	ns	*	0.718	-2.066	-2.784
6	Q9NZZ3;Q9NZZ3-2	CHMP5	*	ns	*	-0.231	-1.695	-1.464
7	Q9Y3Y2-4;Q9Y3Y2;Q9Y3Y2-3	CHTOP	*	ns	*	0.558	3.423	2.864
8	Q99715;Q99715-4;Q99715-2	COL12A1	*	*	*	-0.540	-1.581	-1.041
9	P12111;P12111-2;P12111-4; P12111-5;P12111-3	COL6A3	*	*	ns	-0.380	-0.950	-0.570
10	P29279;P29279-2	CTGF	*	ns	*	-0.595	2.859	3.454
11	O00622	CYR61	*	ns	*	-0.107	1.719	1.826
12	Q6UVK1	CSPG4	*	ns	ns	-0.357	-0.929	-0.572
13	Q5VWQ8-3;Q5VWQ8-4;Q5VWQ8-2; Q5VWQ8-5;Q9UJF2; Q5VWQ8;Q9UJF2-2	DAB2IP;RASAL2	*	ns	*	-0.916	1.236	2.152
14	Q92499;Q92499-3;Q92499-2	DDX1	*	ns	*	0.050	1.250	1.200
15	Q92841;Q92841-1;Q92841-3; Q92841-2	DDX17	*	ns	*	0.367	1.431	1.064
16	Q9NR30;Q9NR30-2;Q9BQ39	DDX21	*	ns	*	0.272	3.135	2.863
17	Q9P265	DIP2B	*	ns	*	0.273	-3.455	-3.728
18	P26358-2;P26358;P26358-3	DNMT1	*	ns	*	-0.449	3.174	3.624
19	O43854-2;O43854	EDIL3	*	ns	*	-0.773	-1.820	-1.046
20	P26641;P26641-2	EEF1G	*	*	ns	0.402	0.755	0.353
21	O00303	EIF3F	*	ns	ns	0.567	1.296	0.729
22	Q9Y6C2;Q9Y6C2-2	EMILIN1	*	ns	*	-0.036	-1.501	-1.465
23	Q52LJ0-1;Q52LJ0	FAM98B	*	ns	*	0.566	2.812	2.246
24	P62942	FKBP1A	*	ns	*	0.214	-2.979	-3.194
25	P35637-2;P35637	FUS	*	ns	*	0.227	1.378	1.151
26	P51114;P51114-3;P51114-2	FXR1	*	ns	*	0.531	2.572	2.041
27	P51116	FXR2	*	ns	*	0.684	3.722	3.038
28	P17302	GJA1	*	ns	*	-0.818	-3.718	-2.900
29	Q92896;Q92896-3;Q92896-2	GLG1	*	ns	*	-0.224	-1.125	-0.900
30	P63244	GNB2L1	*	**	*	0.631	1.189	0.557
31	P29084	GTF2E2	*	ns	*	0.938	4.489	3.550
32	Q8IUE6;Q71UI9-5	HIST2H2AB	*	ns	*	0.389	-2.047	-2.437
33	P01889	HLA-B	*	ns	*	-0.444	-2.192	-1.748
34	Q13151	HNRNPA0	*	ns	*	0.890	3.425	2.535
35	P09651-3;P09651-2;P09651;Q32P51	HNRNPA1;HNRNPA1L2	*	ns	*	0.204	1.009	0.805
36	P22626;P22626-2	HNRNPA2B1	*	ns	*	0.169	0.761	0.592
37	P51991	HNRNPA3	*	ns	*	-0.026	0.990	1.016
38	Q14103-3;Q14103;Q14103-4; Q14103-2	HNRNPD	*	*	*	0.348	0.991	0.642
39	O43390;O43390-3	HNRNPR	*	ns	*	0.203	1.845	1.642
40	Q5SSJ5;Q5SSJ5-3;Q5SSJ5-2; Q5SSJ5-5	HP1BP3	*	ns	*	0.392	-1.463	-1.855

Table 3. continued

#	Protein IDs	Gene names	ANOVA Post-hoc significance			Log2 fold change		
			CTRL vs VEH	CTRL vs HC	VEH vs HC	CTRL vs VEH	CTRL vs HC	VEH vs HC
41	Q0VDF9	HSPA14	*	ns	*	0.490	2.277	1.787
42	P98160	HSPG2	*	ns	*	-0.136	-1.221	-1.085
43	Q16666-3;Q16666-2;Q16666; Q16666-6;Q6K0P9-6;Q6K0P9-5; Q6K0P9-4;Q6K0P9-3;Q6K0P9-2; Q6K0P9	IFI16	*	ns	*	-0.400	3.619	4.020
44	Q9NZI8;Q9NZI8-2	IGF2BP1	*	ns	*	-0.557	3.187	3.744
45	Q9Y6M1-1;Q9Y6M1;Q9Y6M1-5; Q9Y6M1-6;Q9Y6M1-3;Q9Y6M1-4	IGF2BP2	*	ns	*	-0.332	2.963	3.296
46	Q969P0;Q969P0-3;Q969P0-2	IGSF8	*	ns	*	0.303	-1.213	-1.516
47	P53990-2;P53990-3;P53990; P53990-4;P53990-5	IST1	*	*	ns	-0.869	-1.979	-1.110
48	Q6NYC1-2;Q6NYC1;Q6NYC1-3	JMJD6	*	ns	*	-0.343	1.845	2.188
49	Q16363-2;Q16363	LAMA4	*	ns	*	-0.334	-0.888	-0.554
50	Q6PKG0;Q6PKG0-3;Q659C4-7; Q659C4-6;Q659C4-5;Q659C4-2; Q659C4;Q659C4-9	LARP1	*	ns	*	0.657	3.122	2.465
51	Q4G0J3-3;Q4G0J3;Q4G0J3-2	LARP7	*	ns	*	0.183	3.079	2.896
52	P09382	LGALS1	*	ns	*	-0.235	-1.297	-1.062
53	Q9NX58	LYAR	*	ns	*	0.620	4.227	3.607
54	Q9UNF1-2;Q9UNF1;Q12816-5; Q12816-2;Q12816-4;Q12816	MAGED2	*	ns	*	1.430	3.711	2.281
55	Q7Z304	MAMDC2	*	ns	*	-0.173	-2.661	-2.488
56	P29966	MARCKS	*	ns	*	-0.247	-1.399	-1.152
57	Q08431;Q08431-3;Q08431-4; Q08431-2	MFGE8	*	ns	*	-0.275	-1.298	-1.023
58	Q9HCE1;Q9HCE1-2	MOV10	*	ns	*	-0.353	1.751	2.104
59	P19338	NCL	*	ns	*	-0.067	2.023	2.089
60	Q14112-2;Q14112	NID2	*	ns	*	-0.255	-1.501	-1.247
61	Q8TAD7	OCC1	*	ns	*	-0.218	-1.280	-1.061
62	P11940;P11940-2;Q9H361;Q4VXU2; Q4VXU2-2;Q96DU9-2;Q96DU9; Q5JQF8	PABPC1	*	ns	*	0.292	1.328	1.035
63	Q13310-2;Q13310;Q13310-3	PABPC4	*	ns	*	0.021	1.625	1.604
64	P09874	PARP1	*	ns	*	0.269	1.497	1.228
65	Q8WUM4-2;Q8WUM4;Q8WUM4-3	PDCD6IP	*	ns	*	-0.223	-1.054	-0.831
66	P30086	PEBP1	*	ns	*	-0.048	-1.851	-1.804
67	Q8IWS0;Q8IWS0-5;Q8IWS0-3; Q8IWS0-4;Q8IWS0-2	PHF6	*	ns	*	-0.449	4.134	4.583
68	O15031	PLXNB2	*	ns	*	-0.542	-1.175	-0.634
69	Q9NRX1	PNO1	*	ns	*	1.221	3.484	2.264
70	P48634-2;P48634-3;P48634;P48634-4	PRRC2A	*	ns	*	-0.897	3.855	4.752
71	Q9Y520-3;Q9Y520-4;Q9Y520-5; Q9Y520;Q9Y520-7;Q9Y520-2; Q9Y520-6	PRRC2C	*	ns	*	-0.260	3.920	4.180
72	O95084-2;O95084	PRSS23	*	ns	*	-0.270	-1.564	-1.295
73	O75475;O75475-3;O75475-2	PSIP1	*	ns	*	0.009	3.230	3.221
74	Q8IY67-2;Q8IY67;Q8IY67-3	RAVER1	*	ns	*	-0.587	2.153	2.739
75	P38159;P38159-2;Q96E39; P38159-3;O75526;Q8N7X1	RBMX;RBMXL1	*	**	*	0.906	2.826	1.920
76	P62906	RPL10A	*	ns	*	0.300	1.820	1.520
77	P18621-3;P18621;P18621-2	RPL17	*	ns	*	0.131	1.629	1.497

Table 3. continued

#	Protein IDs	Gene names	ANOVA Post-hoc significance			Log2 fold change		
			CTRL vs VEH	CTRL vs HC	VEH vs HC	CTRL vs VEH	CTRL vs HC	VEH vs HC
78	Q07020-2;Q07020	RPL18	*	ns	*	0.217	1.532	1.316
79	P84098	RPL19	*	ns	*	0.081	1.816	1.736
80	P46778	RPL21	*	ns	*	0.247	1.390	1.143
81	P61353	RPL27	*	ns	*	0.246	1.315	1.069
82	P62888	RPL30	*	ns	*	0.474	1.412	0.938
83	P62910	RPL32	*	ns	*	0.294	1.552	1.258
84	P05387;P05386-2	RPLP2	*	ns	*	0.264	1.010	0.746
85	P46783;Q9NQ39	RPS10;RPS10P5	*	ns	*	0.292	1.618	1.326
86	P62280	RPS11	*	ns	*	0.076	1.168	1.092
87	P25398	RPS12	*	ns	*	0.282	1.483	1.202
88	P62263	RPS14	*	ns	*	0.490	2.135	1.645
89	P62841	RPS15	*	ns	*	0.102	1.724	1.622
90	P62249	RPS16	*	ns	*	0.474	1.534	1.060
91	P15880	RPS2	*	ns	*	0.090	1.153	1.062
92	P60866;P60866-2	RPS20	*	ns	*	0.002	1.631	1.629
93	P62847-2;P62847-3;P62847;P62847-4	RPS24	*	*	*	0.635	2.067	1.432
94	P62854;Q5JNZ5	RPS26;RPS26P11	*	ns	*	0.258	1.665	1.407
95	P61247	RPS3A	*	ns	*	0.300	1.505	1.205
96	P46782	RPS5	*	ns	*	0.235	1.634	1.399
97	P08865	RPSA	*	ns	*	0.205	1.116	0.910
98	Q9P2E9;Q9P2E9-3;Q8N4C6-6;Q8N4C6-11	RRBP1	*	ns	*	-0.321	1.021	1.343
99	O43290	SART1	*	ns	*	-0.865	2.419	3.284
100	Q99590-2;Q99590	SCAF11	*	ns	*	-0.198	2.483	2.681
101	O00560-2	SDCBP	*	ns	*	-0.061	-1.341	-1.280
102	P34897-3;P34897;P34897-2	SHMT2	*	ns	*	-0.095	-1.960	-1.864
103	Q9NUQ6;Q9NUQ6-2;Q9NUQ6-4;Q9NUQ6-3	SPATS2L	*	ns	*	-0.478	3.162	3.639
104	P37108	SRP14	*	ns	*	-0.187	1.316	1.503
105	Q08945	SSRP1	*	ns	*	0.717	2.184	1.467
106	O95793-2;O95793;O95793-3	STAU1	*	ns	*	0.610	2.728	2.118
107	O60506-3;O60506;O60506-4;O60506-2;O60506-5	SYNCRIP	*	*	*	0.279	1.283	1.004
108	P35442	THBS2	*	ns	*	-0.393	-1.363	-0.970
109	Q96EY4	TMA16	*	ns	*	-2.328	1.574	3.902
110	P62328	TMSB4X	*	ns	*	-0.110	-1.232	-1.122
111	Q99816;Q99816-2	TSG101	*	*	ns	-0.764	-1.378	-0.614
112	O43657	TSPAN6	*	ns	*	-0.150	-1.767	-1.617
113	Q9C0H2-3;Q9C0H2-2;Q9C0H2;Q9C0H2-4	TTYH3	*	ns	*	-0.530	-4.459	-3.928
114	P67809;Q9Y2T7	YBX1	*	ns	*	0.337	1.337	1.000
115	P16989-2	YBX3	*	ns	*	1.562	4.869	3.308
116	P16989;P16989-3	YBX3	*	ns	*	0.767	4.128	3.361
117	Q6DD87	ZNF787	*	ns	*	0.992	3.983	2.991

4.5 Helium conditioning might reduce mEV secretion of neonatal rat cardiac fibroblasts

EVs play roles in CVD development as well as in cardioprotective mechanisms. To further understand the role of EVs in maintaining the cardiovascular homeostasis, we analyzed the effect of HeC on CF mEVs.

Marek Jelemenský previously demonstrated that HeC increases the migration of NRCFs [66]. During my thesis work, we investigated, how HeC affects EV secretion of these cells. We applied HeC treatment on NRCFs and 40 hours later we isolated mEVs with differential centrifugation from the FBS-free cell culture medium (Figure 5A).

To test the quality of our EV isolates, according to the international standards [25], we characterized mEVs with TEM, western blotting and NTA and Marek Jelemenský preformed flow cytometry. As expected, TEM images revealed membrane particles with 50-200 nm in diameter. Besides, electron dense structures, possibly protein aggregates, which are common contaminants of EV isolates, were also identified (Figure 5B).

Western blot was used to analyze the protein composition of mEV isolates. We detected EV cargo protein Annexin A1 [119] (Figure 5D), however GAPDH, which can accumulate in EVs [119], was below the detection limit. The samples were also negative for markers of potential contaminant, such as ATP5A, Na-K-ATPase and Histone H3. Additionally, fibroblast markers, such as Discoidin domain-containing receptor 2 and Thy-1 membrane glycoprotein were detected on our mEVs with flow cytometry by Marek Jelemenský [66]. Finally, using NTA, we identified particles with diameters ranging from 50 to 700 nm (Figure 5C) that aligns with the expected size range of mEVs. These results confirm that we successfully isolated mEVs of NRCFs with minor protein contamination.

Upon analyzing the particle concentration of our EV isolate, we observed a slight decrease by HeC treatment, with statistical analysis yielding $p = 0.0742$ (Figure 5C). These results suggest that HeC might reduce mEV secretion of NRCFs, however, further orthogonal measurements or increased sample size are needed to validate this finding.

4.6 Neonatal rat cardiac fibroblasts do not secret angiogenic factors or extracellular vesicles after helium conditioning treatment

Angiogenesis is a crucial mechanism that could enhance regeneration after myocardial infarction. Therefore, we investigated whether NRCFs after HeC treatment could enhance angiogenic potential of endothelial cells via paracrine signaling. To test this, we

transferred the EV-rich cell culture supernatant from HeC or control-treated NRCFs to HUVEC-TERT2 and measured their migration and in vitro tube formation capabilities. We found that migration of HUVEC-TERT2 was not affected by the supernatant of HeC-treated NRCFs (Figure 5E,I,J). Additionally, no difference was observed in the parameters analyzed in the tube formation assay (Figure 5F-H,K). These results suggest that the pro-migratory effects of HeC on NRCFs [66] do not extend to endothelial cells via soluble factors or EVs.

In conclusion, however EVs contribute to cardioprotection in certain interventions [57], our study did not reveal any major effect of HeC on NRCF mEV secretion.

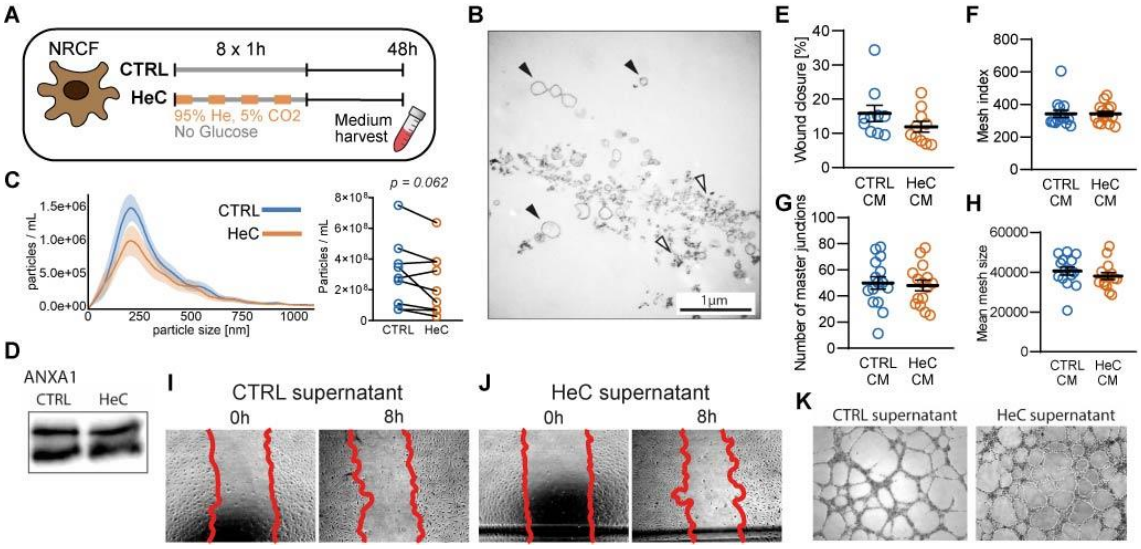

Figure 5.: Analysis on the effect of helium conditioning on cardiac fibroblast extracellular vesicle secretion. *(A) Schematic representation of the experimental plans. NRCF suffered HeC or kept in control conditions and then incubated for 40 hours. Cell culture supernatant was collected for EV isolation and cell treatment. (B) Electron microscopic image of EVs isolated from NRCF cell supernatant. Black arrows: EVs, White arrows: non-vesicular structures. (C) Results of nanoparticle tracking analysis on EV isolates. Left: Particles are ranged from 50-700 nm, right: HeC treatment might reduce the EV secretion of NRCFs. (D) Representative image of Annexin A1 western blot analysis of EV isolates. (E-H) Medium transfer from NRCFs after HeC treatment to HUVEC-TERT2. (E) Cell migration measured by wound healing assay was unaffected by the treatment. No change in (F) tube length, (G) number of nodes and (H) mean mesh size was observed in in vitro tube formation assay. (I-J) Representative images of wound healing assay experiments on HUVEC-TERT2 from cells treated with NRCF supernatant after (I) CTRL or (J) HeC treatment. (K) Representative images of in vitro tube formation assay experiments on HUVEC-TERT2 from cells treated with NRCF supernatant after CTRL or HeC treatment. NRCF: neonatal rat cardiac fibroblast, CTRL: control conditions, HeC: helium conditioning, CM: supernatant from neonatal rat cardiac fibroblast. p represents statistical significance of Wilcoxon's test. Obtained from Jelemenský et. al* [66].

5 Discussion

In this thesis we aimed to investigate the role of EVs in the maintenance of cardiac homeostasis. We hypothesized that HC dysregulates circulating and cardiac-derived EVs and CF-derived EVs contributes to HeC-induced cardioprotection. We identified a difference in the metabolome of pEVs in HC-fed rats. Furthermore, for the first time, we demonstrated that HC dysregulates CM sEV secretion substantially. Regarding to cardioprotective interventions, we observed that HeC do not appear to significantly affect mEVs from CFs. These results demonstrate the potential of EVs in the development of novel diagnostics and therapeutics for CVDs.

5.1 Metabolome of circulating extracellular vesicles in hypercholesterolemia

Previous studies have characterized the proteomics and miRNA profiles of circulating EVs in the context of metabolic disorders [48,50]. Here, we expanded our understanding on how HC affects EVs by analyzing pEVs isolated from rats fed with hypercholesterolemic chow. When we correlated the amount of certain metabolites between plasma and pEV samples, we found only a minor connection. These results strengthen the hypothesis that analyzing EVs can provide novel insight into the analyzed pathophysiological conditions. Such information can be utilized to develop new diagnostic and prognostic measurements for the early identification of maladaptive mechanisms in HC.

We also found that HC significantly reduces the amount of multiple PCs in pEVs. These observations align with the findings of Blandin *et al.,* who reported reduced PC content in EVs isolated from adipocytes of high-fat diet fed mice [120]. As PCs are major constituents of plasma membranes, the impact of such changes on cardiac homeostasis remains uncertain. However, given that EV-transferred metabolites can affect remote tissues [121] and that the amount of certain PCs are dysregulated in other disease states as well [122–124], these changes may contribute to maladaptive processes in HC and CVD development.

In conclusion, our results demonstrate that HC affects the metabolome of pEVs that might play a role in the pathomechanism of CVDs. In addition, these changes could not be identified with the analysis of the plasma alone. Upon these results, future clinical studies

on non-obese, but hypercholesterolemic patients without lipid lowering therapies and corresponding controls should be implemented to investigate whether similar changes can be identified in human pEVs as well.

5.2 Effect of hypercholesterolemia on extracellular vesicle secretion of cardiomyocytes

In our experiments on AC16 cells, we demonstrated that HC elevates the secretion sEV of CMs. Elevated intracellular cholesterol can increase EV secretion through various mechanisms. Strauss *et al.* demonstrated that cholesterol treatment elevates EV secretion of Oli-Neu cells [125]. They suggest that this is a mechanism to eliminate cholesterol from the endosomal/lysosomal system. In accordance with these results, a recent study demonstrates that cholesterol accumulates in EVs via active processes [27]. When cholesterol-rich EVs are secreted, they can act as external cholesterol source for recipient cells. These results suggest that, when cells are in an excess of cholesterol, they may get rid of the surplus via increased EV secretion. Furthermore, cholesterol plays a significant role in lipid raft formation [126], which is involved in EV biogenesis [127], thus elevated number of lipid rafts may also contribute to the increased number of secreted EVs in HC. Taking into account that we observed reduced relative concentration of certain ESCRT complex constituents, which is one of the best known protein complexes involved in exosome and ectosome biogenesis [23], we propose that the elevated EV secretion is mediated by non-canonical, cholesterol-specific EV secretory mechanisms.

On the other hand, we did not observe any differences in the lipid-to-protein ratio or PC concentration of CM sEVs. Similarly, the elasticity of CM sEVs was unaffected by HC. These findings suggest that the membrane composition of CM sEVs is not significantly altered under HC conditions, thus these EVs may be secreted via a mechanism that preserves vesicular membrane composition. In conclusion, we suggest that HC induces pathological EV secretory pathways distinct from those predominant under normal conditions. As such processes may not CM specific, these changes could explain the increased number of circulating EVs in HC. Further investigation into these pathways may lead to the identification of specific EV subpopulations associated to HC and CVDs.

Upon inflammation induced by CM EVs, we initially hypothesized that altered CM EV secretion under HC might activate immune cells. However, our results with THP-ASC-

GFP cells indicate that sEVs derived from HC-treated CMs do not affect cytokine expression and ASC-dependent inflammasome activation in monocytes. This is in line with our proteomics analysis, as we did not observe elevation in any proteins associated with inflammation.

In contrast, we identified numerous proteins associated with the extracellular matrix or cell adhesion that had lower concentrations in CM sEVs in HC. Additionally, numerous proteins associated with tissue remodeling were enriched. These results suggest that CMs secrete EVs that may contribute to cardiac tissue remodeling in HC, potentially leading to cardiac dysfunction.

Moreover, we identified that certain proteins with higher abundance in EVs derived from HC-treated CMs regulate lipid metabolism and adipocyte differentiation. Several studies described that CM EVs establishes communication between cardiac and adipose tissue [128–130]. Therefore, these changes might aim to alleviate dyslipidemia and also indicate the stressed metabolic condition of the CMs.

We also observed elevated amount of CYR61 in CM EVs in HC, similarly to circulating EVs in acute coronary syndrome [131]. Moreover, GJA1 that was reduced in CM EVs in HC is also reduced in circulating and CM EVs after myocardial infarction [132]. Thes findings demonstrate that the dysregulated proteome of CM EVs represents stress signals that are observed in CVDs as well as specific responses to the hypercholesterolemic status of CMs.

Finally, as we observed that many proteins upregulated in HC conditions in CM sEVs can bind RNA and some play a role in EV miRNA packaging, we suggest that HC also affects the RNA composition of CM sEVs.

In conclusion, we identified that HC increases CM EV secretion through pathways that are potentially specific to diseased conditions. Contrary to our hypothesis, HC does not affect the inflammatory potential of CM EVs. However, it significantly affects their proteome and possibly RNA composition. The identified changes suggest that EVs derived from CMs in HC induces cardiac tissue remodeling. To further analyze these results, in vitro and translational experiments will need to be performed. In addition, if CM EVs could be enriched from plasma, analysis of such changes and could be the basis of diagnostic tools to identify the stressed condition of CMs in the early stages of CVD development.

5.3 Effect of helium conditioning on cardiac fibroblast EV secretion

To investigate the role of EVs in a cardioprotective therapy, we applied HeC on CFs and isolated mEVs. Given that EVs are involved in mechanisms activated by certain cardioprotective interventions, such as IPC [57], we hypothesized that HeC modulates CF mEV secretion.

According to our NTA measurements, HeC do not have major effect on the amount of secreted mEVs from CFs. Previously, Jelemenský demonstrated that HeC accelerates NRCF migration, however this effect could not be propagated to un-treated CFs with EV-rich supernatant transfer [66]. Similarly, we observed that, secretome, including EVs, of HeC-treated CFs, do not modulate the function of endothelial cells. Similarly, Smit *et. al* demonstrated that helium treatment has direct effect on endothelial cells, but the observed changes cannot be transferred to naïve cells with supernatant transfer [133]. Considering that HeC modulates EV secretion from various sources [58–60], and EVs are involved in other cardioprotective therapies [57], certain EV subpopulations might play a role in physiological mechanisms related to HeC-induced cardioprotection, however, according to our data, CF-secreted mEVs have a minor role in this context.

Taken together these results we conclude that EVs are involved in maintaining cardiac homeostasis through regulating cardioprotective mechanisms, however, because of the complexity of EVs, specific experiments focusing on EV subpopulations are needed to clearly identify their roles in cardiac physiology.

6 Conclusions

To gain further insight into the role of EVs in cardiac physiology, we examined the effects of both cardiotoxic HC and cardioprotective HeC on EVs. We specifically focused on the metabolome of pEVs in HC and investigated how HC affects CM sEV secretion and whether the changes contribute to inflammation. Furthermore, we analyzed how HeC affects CF mEV secretion and its effect on endothelial function.

Our findings that HC significantly alters metabolome of pEVs, which is regulated differently from the plasma metabolome, strengthens the original hypothesis that analyzing EVs can reveal information about the disease states that would remain hidden if plasma metabolome was investigated alone. Furthermore, considering that HC dysregulates circulating EV proteome and miRNA composition as well [48,50], we conclude that HC greatly impacts the molecular composition of pEVs, which may play a role in CVD development and such changes can be the basis of future diagnostic tools.

Moreover, we demonstrated that HC increases CM sEV secretion. However, unlike in other stressed conditions, such as hypertrophy [54], EVs derived from hypercholesterolemic CMs do not modulate immune cells. Instead, they may induce cardiac tissue remodeling and potentially regulate gene expression of adipose tissue. Together with our results on pEVs, we conclude that EVs can play significant role in altered intercellular communication in HC. The identified changes can regulate intracardiac and systemic changes to maintain the homeostasis of the body.

In contrast to our results in HC conditions, we observed limited effect of HeC on CF mEVs. While HeC might slightly affect the quantity of secreted mEVs, the vesicles do not transmit activation signals to endothelial cells. Taking into account that EVs play significant roles in other cardioprotective mechanisms, such as IPC [57], and that HeC affects EVs from certain sources [58–60], we suggest that EVs are involved in cardioprotective mechanisms, however CF mEVs have limited role in HeC.

In conclusion, in this thesis we demonstrate that EVs are important players in conditions with high cardiovascular risks, such as HC. Furthermore, EVs are also involved in certain cardioprotective mechanisms. These results demonstrate that EVs contribute to cardiac homeostasis and further understanding of their functional roles can facilitate the development of novel diagnostics and therapeutics for CVDs. Our observations, such as the neutral effect of HeC on CM EVs, highlights the complexity of EV-mediated

transcellular communication as well. To fully understand the role of EVs in CVD progression, future experiments with specific focus on subpopulations of EVs, including detailed analysis of EV composition and function need to be implemented. These small, targeted steps will take us to the final understanding of what EVs do to keep the heart and our body healthy.

7 Summary

CVDs are the leading cause of deaths worldwide [2], indicating an incomplete understanding of their pathomechanism. A major comorbidity of CVDs is metabolic diseases, including HC [2]. EVs are nano-sized, cell-secreted membrane particles [23], involved in HC, CVDs and cardioprotective therapies [35–37,57]. However, their role in cardiovascular homeostasis is yet unclear.

This thesis aims to elucidate the role of EVs in cardiac stress responses by examining the effect of a cardiotoxic condition, HC, and a cardioprotective intervention, HeC, on EVs. Specifically, the objectives are to: 1) analyze how HC modifies the metabolome of circulating EVs, 2) determine how HC regulates CM EV secretion, 3) investigate whether CM EVs in HC induce inflammation, and 4) examine how HeC modifies NRCF EV secretion.

pEVs were isolated from male Wistar Rats fed with hypercholesterolemic chow and their metabolome was analyzed using the Biocrates MxP Quant 500 kit. Furthermore, AC16 CMs were treated with Remembrane® HC supplement and sEVs were isolated from the cell culture supernatant. AC16 sEVs were quantitatively analyzed, used for THP-1-ASC-GFP monocyte cell treatment, and their proteome was measured with LC-MS/MS. In addition, HeC treatment was applied on CFs, mEVs were isolated, and HUVEC-TERT2 were treated with conditioned CF cell culture supernatant.

We found that HC reduces the amount of certain glycerophospholipids in pEVs. Furthermore, the metabolome of pEVs showed only minor correlation with plasma metabolome. HC treatment increased AC16 sEV secretion, however sEVs from neither experimental group activated monocytes. On the other hand, proteomics of AC16 sEVs revealed significant effects of HC, and certain proteins involved in in cardiac tissue remodeling found enriched. HeC had no major effect on CF mEV secretion, and supernatant transfer from HeC-treated CFs to HUVEC-TERT2 did not affect recipient cell function.

In conclusion, HC alters the composition and potentially the function of both circulating and CM-derived EVs. Furthermore, CF EVs do not play major role in HeC. Our results demonstrates that EVs are involved in the regulation of cardiac homeostasis. For complete understanding of these mechanisms, experiments with specific focus on subpopulations of EVs are needed.

8 References

1. Mensah GA, Fuster V, Murray CJL, Roth GA. Global Burden of Cardiovascular Diseases and Risks, 1990-2022. J Am Coll Cardiol. 2023 Dec 19;82(25):2350–2473.
2. Murray CJL. The Global Burden of Disease Study at 30 years. Nat Med. 2022;28(10):2019–2026.
3. Heusch G. Myocardial ischaemia–reperfusion injury and cardioprotection in perspective. Nat Rev Cardiol [Internet]. 2020;17(12):773–789. Available from: http://dx.doi.org/10.1038/s41569-020-0403-y
4. Murry CE, Jennings RB, Reimer KA. Preconditioning with ischemia: A delay of lethal cell injury in ischemic myocardium. Circulation. 1986;74(5):1124–1136.
5. Sayour N V., Brenner GB, Makkos A, Kiss B, Kovácsházi C, Gergely TG, Aukrust SG, Tian H, Zenkl V, Gömöri K, Szabados T, Bencsik P, Heinen A, Schulz R, Baxter GF, Zuurbier CJ, Vokó Z, Ferdinandy P, Giricz Z. Cardioprotective efficacy of limb remote ischaemic preconditioning in rats: discrepancy between a meta-analysis and a three-centre in vivo study. Cardiovasc Res [Internet]. 2023;119(6):1336–1151. Available from: https://doi.org/10.1093/cvr/cvad024
6. García del Blanco B, Otaegui I, Rodríguez-Palomares JF, Bayés-Genis A, Fernández-Nofrerías E, Vilalta del Olmo V, Carrillo X, Ibáñez B, Worner F, Casanova J, Pueo E, González-Juanatey JR, López-Pais J, Bardají A, Bonet G, Fuertes M, Rodríguez-Sinovas A, Ruiz-Meana M, Inserte J, Barba I, Gómez-Talavera S, Martí G, Serra B, Bellera N, Ojeda-Ramos M, Cuellar H, Valente F, Carmona MÁ, Miró-Casas E, Marsal JR, Sambola A, Lidón RM, Bañeras J, Elízaga J, Padilla F, Barrabés JA, Hausenloy DJ, Ferreira-González I, García-Dorado D. Effect of COMBinAtion therapy with remote ischemic conditioning and exenatide on the Myocardial Infarct size: a two-by-two factorial randomized trial (COMBAT-MI). Basic Res Cardiol [Internet]. 116(1):1–12. Available from: https://link.springer.com/article/10.1007/s00395-021-00842-2
7. Hausenloy DJ, Kharbanda RK, Møller UK, Ramlall M, Aarøe J, Butler R, Bulluck H, Clayton T, Dana A, Dodd M, Engstrom T, Evans R, Lassen JF, Christensen EF, Garcia-Ruiz JM, Gorog DA, Hjort J, Houghton RF, Ibanez B, Knight R, Lippert FK, Lønborg JT, Maeng M, Milasinovic D, More R, Nicholas JM, Jensen LO,

Perkins A, Radovanovic N, Rakhit RD, Ravkilde J, Ryding AD, Schmidt MR, Riddervold IS, Sørensen HT, Stankovic G, Varma M, Webb I, Terkelsen CJ, Greenwood JP, Yellon DM, Bøtker HE. Effect of remote ischaemic conditioning on clinical outcomes in patients with acute myocardial infarction (CONDI-2/ERIC-PPCI): a single-blind randomised controlled trial. Lancet [Internet]. 2019 Oct 19 [cited 2021 Sep 21];394(10207):1415–1424. Available from: http://www.thelancet.com/article/S0140673619320392/fulltext

8. De Deken J, Rex S, Monbaliu Di, Pirenne J, Jochmans I. The Efficacy of Noble Gases in the Attenuation of Ischemia Reperfusion Injury: A Systematic Review and Meta-Analyses. Crit Care Med. 2016;44(9):886–896.
9. Smit KF, Weber NC, Hollmann MW, Preckel B. Noble gases as cardioprotectants - Translatability and mechanism. Br J Pharmacol. 2015;172(8):2062–2073.
10. Pagel PS. Cardioprotection by Noble Gases. J Cardiothorac Vasc Anesth [Internet]. 2010;24(1):143–163. Available from: http://dx.doi.org/10.1053/j.jvca.2009.03.016
11. Pagel PS, Krolikowski JG, Shim YH, Venkatapuram S, Kersten JR, Weihrauch D, Warltier DC, Pratt PF. Noble gases without anesthetic properties protect myocardium against infarction by activating prosurvival signaling kinases and inhibiting mitochondrial permeability transition in vivo. Anesth Analg. 2007;105(3):562–569.
12. Huhn R, Heinen A, Weber NC, Hieber S, Hollmann MW, Schlack W, Preckel B. Helium-induced late preconditioning in the rat heart in vivo. Br J Anaesth [Internet]. 2009;102(5):614–619. Available from: http://dx.doi.org/10.1093/bja/aep042
13. Pagel PS, Krolikowski JG, Pratt PF, Shim YH, Amour J, Warltier DC, Weihrauch D. The mechanism of helium-induced preconditioning: A direct role for nitric oxide in rabbits. Anesth Analg [Internet]. 2008 [cited 2024 May 24];107(3):762–768. Available from: https://journals.lww.com/anesthesia-analgesia/fulltext/2008/09000/the_mechanism_of_helium_induced_preconditioning__a.8.aspx
14. Heinen A, Huhn R, Smeele KMA, Zuurbier CJ, Schlack W, Preckel B, Weber NC, Hollmann MW. Helium-induced Preconditioning in Young and Old Rat Heart:

Impact of Mitochondrial Ca2+-sensitive Potassium Channel Activation. Anesthesiology. 2008;109(5):830–836.

15. Andersson C, Johnson AD, Benjamin EJ, Levy D, Vasan RS. 70-year legacy of the Framingham Heart Study. Nat Rev Cardiol [Internet]. 2019;16(11):687–698. Available from: http://dx.doi.org/10.1038/s41569-019-0202-5
16. Andreadou I, Iliodromitis EK, Lazou A, Görbe A, Giricz Z, Schulz R, Ferdinandy P. Effect of hypercholesterolaemia on myocardial function, ischaemia–reperfusion injury and cardioprotection by preconditioning, postconditioning and remote conditioning. Br J Pharmacol [Internet]. 2017 Jun 1 [cited 2021 Aug 24];174(12):1555–1569. Available from: https://bpspubs.onlinelibrary.wiley.com/doi/full/10.1111/bph.13704
17. Ónody A, Csonka C, Giricz Z, Ferdinandy P. Hyperlipidemia induced by a cholesterol-rich diet leads to enhanced peroxynitrite formation in rat hearts. Cardiovasc Res. 2003;58(3):663–670.
18. Huang Y, Walker KE, Hanley F, Narula J, Houser SR, Tulenko TN. Cardiac Systolic and Diastolic Dysfunction after a Cholesterol-Rich Diet. Circulation. 2004;109(1):97–102.
19. Varga Z V., Kupai K, Szucs G, Gáspár R, Pálóczi J, Faragó N, Zvara Á, Puskás LG, Rázga Z, Tiszlavicz L, Bencsik P, Görbe A, Csonka C, Ferdinandy P, Csont T. MicroRNA-25-dependent up-regulation of NADPH oxidase 4 (NOX4) mediates hypercholesterolemia-induced oxidative/nitrative stress and subsequent dysfunction in the heart. J Mol Cell Cardiol. 2013;62:111–121.
20. Giricz Z, Lalu MM, Csonka C, Bencsik P, Schulz R, Ferdinandy P. Hyperlipidemia Attenuates the Infarct Size-Limiting Effect of Ischemic Preconditioning: Role of Matrix Metalloproteinase-2 Inhibition. J Pharmacol Exp Ther [Internet]. 2006 Jan 1 [cited 2024 Jul 18];316(1):154–161. Available from: https://jpet.aspetjournals.org/content/316/1/154
21. Szilvassy Z, Ferdinandy P, Szilvassy J, Nagy I, Karcsu S, Lonovics J, Dux L, Koltai M. The loss of pacing-induced preconditioning in atherosclerotic rabbits: Role of hypercholesterolaemia. J Mol Cell Cardiol. 1995;27(12):2559–2569.
22. Ferdinandy P, Hausenloy DJ, Heusch G, Baxter GF, Schulz R. Interaction of risk factors, comorbidities, and comedications with ischemia/reperfusion injury and

cardioprotection by preconditioning, postconditioning, and remote conditioning. Pharmacol Rev. 2014 Oct;66(4):1142–1174.

23. van Niel G, D'Angelo G, Raposo G. Shedding light on the cell biology of extracellular vesicles. Nat Rev Mol Cell Biol [Internet]. 2018;19(4):213–228. Available from: http://www.ncbi.nlm.nih.gov/pubmed/29339798
24. Buzas EI. The roles of extracellular vesicles in the immune system. Nat Rev Immunol. 2022;23(April).
25. Joshua A. Welsh, Deborah C.I. Goberdhan, Lorraine O'Driscol, Edit I. Buzas, Cherie Blenkiron, Benedetta Bussolati, Houjian Cai, Dolores Di Vizio, Tom A.P. Driedonks, Uta Erdbrügger, Juan M. Falcon-Perez, Qing-Ling Fu, Andrew F. Hill, Metka Lenassi SK, Lim, Mỹ G. Mahoney, Sujata Mohanty, Andreas Möller, Rienk Nieuwland, Takahiro Ochiya, Susmita Sahoo, Ana C. Torrecilhas, Lei Zheng, Andries Zijlstra, Paolo Bergese, Esther M Bridges, Marco Brucale, Dylan Burger, Randy P. Carney, Federico Cocozza, Emanuele KWW. Minimal information for studies of extracellular vesicles (MISEV2023): from basic to advanced approaches. J Extracell Vesicles. 2023;12(12).
26. Garcia-Martin R, Wang G, Brandão BB, Zanotto TM, Shah S, Kumar Patel S, Schilling B, Kahn CR. MicroRNA sequence codes for small extracellular vesicle release and cellular retention. Nature. 2022;601(7893):446–451.
27. Palmulli R, Couty M, Piontek MC, Ponnaiah M, Dingli F, Verweij FJ, Charrin S, Tantucci M, Sasidharan S, Rubinstein E, Kontush A, Loew D, Lhomme M, Roos WH, Raposo G, van Niel G. CD63 sorts cholesterol into endosomes for storage and distribution via exosomes. Nat Cell Biol [Internet]. 2024;26(July). Available from: http://dx.doi.org/10.1038/s41556-024-01432-9
28. Lee YJ, Shin KJ, Chae YC. Regulation of cargo selection in exosome biogenesis and its biomedical applications in cancer. Exp Mol Med. 2024;56(4):877–889.
29. Munir J, Yoon JK, Ryu S. Therapeutic miRNA-Enriched Extracellular Vesicles: Current Approaches and Future Prospects. Cells 2020, Vol 9, Page 2271 [Internet]. Available from: https://www.mdpi.com/2073-4409/9/10/2271/htm
30. Margolis E, Brown G, Partin A, Carter B, McKiernan J, Tutrone R, Torkler P, Fischer C, Tadigotla V, Noerholm M, Donovan MJ, Skog J. Predicting high-grade prostate cancer at initial biopsy: clinical performance of the ExoDx (EPI) Prostate

Intelliscore test in three independent prospective studies. Prostate Cancer Prostatic Dis [Internet]. 2022;25(2):296–301. Available from: http://dx.doi.org/10.1038/s41391-021-00456-8

31. Tutrone R, Lowentritt B, Neuman B, Donovan MJ, Hallmark E, Cole TJ, Yao Y, Biesecker C, Kumar S, Verma V, Sant GR, Alter J, Skog J. ExoDx prostate test as a predictor of outcomes of high-grade prostate cancer – an interim analysis. Prostate Cancer Prostatic Dis. 2023;26(3):596–601.
32. Bonsergent E, Grisard E, Buchrieser J, Schwartz O, Théry C, Lavieu G. Quantitative characterization of extracellular vesicle uptake and content delivery within mammalian cells. Nat Commun ;12(1):1–11. Available from: http://dx.doi.org/10.1038/s41467-021-22126-y
33. Das D, Jothimani G, Banerjee A, Dey A, Duttaroy AK, Pathak S. A brief review on recent advances in diagnostic and therapeutic applications of extracellular vesicles in cardiovascular disease. Int J Biochem Cell Biol. 2024 Aug 1;173:106616.
34. Wu R, Hu X, Wang J. Current optimized strategies for stem cell-derived extracellular vesicle/exosomes in cardiac repair. J Mol Cell Cardiol. 2023 Nov 1;184:13–25.
35. Sluijter JPG, Davidson SM, Boulanger CM, Buzás EI, de Kleijn DPV, Engel FB, Giricz Z, Hausenloy DJ, Kishore R, Lecour S, Leor J, Madonna R, Perrino C, Prunier F, Sahoo S, Schiffelers RM, Schulz R, Van Laake LW, Ytrehus K, Ferdinandy P. Extracellular vesicles in diagnostics and therapy of the ischaemic heart: Position Paper from the Working Group on Cellular Biology of the Heart of the European Society of Cardiology. Cardiovasc Res [Internet]. 2018;114(1):19–34. Available from: http://www.ncbi.nlm.nih.gov/pubmed/29106545%0Ahttp://www.pubmedcentral.nih.gov/articlerender.fcgi?artid=PMC5852624
36. Akbar N, Azzimato V, Choudhury RP, Aouadi M. Extracellular vesicles in metabolic disease. Diabetologia [Internet];62(12):2179–2187. Available from: /pmc/articles/PMC6861353/
37. Martínez MC, Andriantsitohaina R. Extracellular vesicles in metabolic syndrome. Circ Res [Internet];120(10):1674–1686. Available from:

https://www.ahajournals.org/doi/abs/10.1161/CIRCRESAHA.117.309419

38. Davidson SM, Riquelme JA, Takov K, Vicencio JM, Boi-Doku C, Khoo V, Doreth C, Radenkovic D, Lavandero S, Yellon DM. Cardioprotection mediated by exosomes is impaired in the setting of type II diabetes but can be rescued by the use of non-diabetic exosomes in vitro. J Cell Mol Med. 2018;22(1):141–151.
39. Gan L, Xie D, Liu J, Bond Lau W, Christopher TA, Lopez B, Zhang L, Gao E, Koch W, Ma XL, Wang Y. Small Extracellular Microvesicles Mediated Pathological Communications between Dysfunctional Adipocytes and Cardiomyocytes as a Novel Mechanism Exacerbating Ischemia/Reperfusion Injury in Diabetic Mice. Circulation. 2020;968–983.
40. Zhao X, Si L, Bian J, Pan C, Guo W, Qin P, Zhu W, Xia Y, Zhang Q, Wei K. Adipose tissue macrophage-derived exosomes induce ferroptosis via glutathione synthesis inhibition by targeting SLC7A11 in obesity-induced cardiac injury. Free Radic Biol Med [Internet]. 2022;182(February):232–245. Available from: https://doi.org/10.1016/j.freeradbiomed.2022.02.033
41. Heinrich LF, Andersen DK, Cleasby ME, Lawson C. Long-term high fat feeding of rats results in increased numbers of circulating microvesicles with pro-inflammatory effects on endothelial cells. Br J Nutr. 2015;113(11):1704–1711.
42. Rigamonti AE, Bollati V, Pergoli L, Iodice S, De Col A, Tamini S, Cicolini S, Tringali G, De Micheli R, Cella SG, Sartorio A. Effects of an acute bout of exercise on circulating extracellular vesicles: tissue-, sex-, and BMI-related differences. Int J Obes. 2020;44(5):1108–1118.
43. Ali S, Malloci M, Safiedeen Z, Soleti R, Vergori L, Vidal-Gómez X, Besnard C, Dubois S, Le Lay S, Boursier J, Chevrollier A, Gagnadoux F, Simard G, Andriantsitohaina R, Martinez MC. LPS-enriched small extracellular vesicles from metabolic syndrome patients trigger endothelial dysfunction by activation of TLR4. Metabolism. 2021;118.
44. Suades R, Padró T, Alonso R, López-Miranda J, Mata P, Badimon L. Circulating CD45+/CD3+ lymphocyte-derived microparticles map lipid-rich atherosclerotic plaques in familial hypercholesterolaemia patients. Thromb Haemost. 2013;111(1):111–121.
45. Nielsen MH, Irvine H, Vedel S, Raungaard B, Beck-Nielsen H, Handberg A. The

Impact of Lipoprotein-Associated Oxidative Stress on Cell-Specific Microvesicle Release in Patients with Familial Hypercholesterolemia. Oxid Med Cell Longev. 2016;2016.

46. Chiva-Blanch G, Padró T, Alonso R, Crespo J, Perez De Isla L, Mata P, Badimon L. Liquid Biopsy of Extracellular Microvesicles Maps Coronary Calcification and Atherosclerotic Plaque in Asymptomatic Patients with Familial Hypercholesterolemia: A Computed Tomographic Angiography Imaging Study. Arterioscler Thromb Vasc Biol. 2019 May 1;39(5):945–955.
47. Suades R, Padró T, Crespo J, Sionis A, Alonso R, Mata P, Badimon L. Liquid Biopsy of Extracellular Microvesicles Predicts Future Major Ischemic Events in Genetically Characterized Familial Hypercholesterolemia Patients. Arterioscler Thromb Vasc Biol. 2019;39(6):1172–1181.
48. Barrachina MN, Sueiro AM, Casas V, Izquierdo I, Hermida-Nogueira L, Guitián E, Casanueva FF, Abián J, Carrascal M, Pardo M, García Á. A Combination of Proteomic Approaches Identifies A Panel of Circulating Extracellular Vesicle Proteins Related to the Risk of Suffering Cardiovascular Disease in Obese Patients. Proteomics. 2019;19(1–2):1–10.
49. Vilahur G, Ben-Aicha S, Badimon L. New insights into the role of adipose tissue in thrombosis. Cardiovasc Res. 2017;113(9):1046–1054.
50. Kim H, Bae YU, Lee H, Kim H, Jeon JS, Noh H, Han DC, Byun DW, Kim SH, Park HK, Ryu S, Kwon SH. Effect of diabetes on exosomal miRNA profile in patients with obesity. BMJ Open Diabetes Res Care. 2020;8(1):1–8.
51. Collado A, Domingo E, Piqueras L, Sanz MJ. Primary hypercholesterolemia and development of cardiovascular disorders: Cellular and molecular mechanisms involved in low-grade systemic inflammation and endothelial dysfunction. Int J Biochem Cell Biol [Internet] Available from: https://doi.org/10.1016/j.biocel.2021.106066
52. Fandl HK, Garcia VP, Treuth JW, Brewster LM, Greiner JJ, Davy KP, Stauffer BL, Desouza CA. Endothelial-derived extracellular vesicles from obese/hypertensive adults increase factors associated with hypertrophy and fibrosis in cardiomyocytes. Am J Physiol - Hear Circ Physiol. 2023;324(5):H675–685.

53. Li J, Zhang Q, Jiao H. LncRNA NRON promotes M2 macrophage polarization and alleviates atrial fibrosis through suppressing exosomal miR-23a derived from atrial myocytes. J Formos Med Assoc [Internet]. 2021;120(7):1512–1519. Available from: https://doi.org/10.1016/j.jfma.2020.11.004
54. Yu H, Qin L, Peng Y, Bai W, Wang Z. Exosomes Derived From Hypertrophic Cardiomyocytes Induce Inflammation in Macrophages via miR-155 Mediated MAPK Pathway. Front Immunol. 2021;11(February):1–11.
55. Sun S, Wu Y, Maimaitijiang A, Huang Q, Chen Q. Ferroptotic cardiomyocyte-derived exosomes promote cardiac macrophage M1 polarization during myocardial infarction. PeerJ. 2022;10:1–18.
56. Chen C, Cai S, Wu M, Wang R, Liu M, Cao G, Dong M, Yiu KH. Role of Cardiomyocyte-Derived Exosomal MicroRNA-146a-5p in Macrophage Polarization and Activation. Dis Markers. 2022;2022.
57. Giricz Z, Varga Z V., Baranyai T, Sipos P, Pálóczi K, Kittel Á, Buzás EI, Ferdinandy P. Cardioprotection by remote ischemic preconditioning of the rat heart is mediated by extracellular vesicles. J Mol Cell Cardiol [Internet]. 2014;68:75–78. Available from: http://dx.doi.org/10.1016/j.yjmcc.2014.01.004
58. Weber NC, Schilling JM, Warmbrunn M V., Dhanani M, Kerindongo R, Siamwala J, Song Y, Zemljic-Harpf AE, Fannon MJ, Hollmann MW, Preckel B, Roth DM, Patel HH. Helium-induced changes in circulating caveolin in mice suggest a novel mechanism of cardiac protection. Int J Mol Sci. 2019;20(11):1–18.
59. Thom SR, Bhopale VM, Yang M. Neutrophils generate microparticles during exposure to inert gases due to cytoskeletal oxidative stress. J Biol Chem. 2014;289(27):18831–18845.
60. Smit KF, Kerindongo RP, Böing A, Nieuwland R, Hollmann MW, Preckel B, Weber NC. Effects of helium on inflammatory and oxidative stress-induced endothelial cell damage. Exp Cell Res [Internet]. 2015;337(1):37–43. Available from: http://dx.doi.org/10.1016/j.yexcr.2015.06.004
61. Pinto AR, Ilinykh A, Ivey MJ, Kuwabara JT, D'antoni ML, Debuque R, Chandran A, Wang L, Arora K, Rosenthal NA, Tallquist MD. Revisiting cardiac cellular composition. Circ Res. 2016;118(3):400–409.
62. Talman V, Ruskoaho H. Cardiac fibrosis in myocardial infarction—from repair

and remodeling to regeneration. Cell Tissue Res. 2016;365(3):563–581.

63. Humeres C, Frangogiannis NG. Fibroblasts in the Infarcted, Remodeling, and Failing Heart. JACC Basic to Transl Sci. 2019;4(3):449–467.

64. Quijada P, Trembley MA, Small EM. The Role of the Epicardium During Heart Development and Repair. Circ Res. 2020;126(8):377–394.

65. Frangogiannis NG. Cardiac fibrosis: Cell biological mechanisms, molecular pathways and therapeutic opportunities. Mol Aspects Med. 2019;65(July):70–99.

66. Jelemenský M, Kovácsházi C, Ferenczyová K, Hofbauerová M, Kiss B, Pállinger É, Kittel Á, Sayour VN, Görbe A, Pelyhe C, Hambalkó S, Kindernay L, Barančík M, Ferdinandy P, Barteková M, Giricz Z. Helium conditioning increases cardiac fibroblast migration which effect is not propagated via soluble factors or extracellular vesicles. Int J Mol Sci. 2021;22(19).

67. House SL, Wang J, Castro AM, Weinheimer C, Kovacs A, Ornitz DM. Fibroblast growth factor 2 is an essential cardioprotective factor in a closed-chest model of cardiac ischemia-reperfusion injury. Vol. 3, Physiological Reports. 2015.

68. Seki K, Sanada S, Kudinova AY, Steinhauser ML, Handa V, Gannon J, Lee RT. Interleukin-33 prevents apoptosis and improves survival after experimental myocardial infarction through ST2 signaling. Circ Hear Fail. 2009;2(6):684–691.

69. Abrial M, Da Silva CC, Pillot B, Augeul L, Ivanes F, Teixeira G, Cartier R, Angoulvant D, Ovize M, Ferrera R. Cardiac fibroblasts protect cardiomyocytes against lethal ischemia-reperfusion injury. J Mol Cell Cardiol [Internet]. 2014;68:56–65. Available from: http://dx.doi.org/10.1016/j.yjmcc.2014.01.005

70. Luo H, Li X, Li T, Zhao L, He J, Zha L, Qi Q, Yu Z. Microrna-423-3p exosomes derived from cardiac fibroblasts mediates the cardioprotective effects of ischaemic post-conditioning. Cardiovasc Res. 2019;115(7):1189–1204.

71. Kovácsházi C, Hambalkó S, Sayour N V, Gergely TG, Brenner GB, Pelyhe C, Kapui D, Weber BY, Hültenschmidt AL, Pállinger É, Buzás EI, Zolcsák Á, Kiss B, Bozó T, Csányi C, Kósa N, Kellermayer M, Farkas R, Karvaly GB, Wynne K, Matallanas D, Ferdinandy P. Effect of hypercholesterolemia on circulating and cardiomyocyte - derived extracellular vesicles. Sci Rep [Internet]. 2024;1–14. Available from: https://doi.org/10.1038/s41598-024-62689-6

72. Baranyai T, Herczeg K, Onódi Z, Voszka I, Módos K, Marton N, Nagy G, Mäger

I, Wood MJ, El Andaloussi S, Pálinkás Z, Kumar V, Nagy P, Kittel Á, Buzás EI, Ferdinandy P, Giricz Z. Isolation of exosomes from blood plasma: Qualitative and quantitative comparison of ultracentrifugation and size exclusion chromatography methods. PLoS One. 2015;10(12):1–13.

73. Onódi Z, Pelyhe C, Nagy CT, Brenner GB, Almási L, Kittel Á, Manček-Keber M, Ferdinandy P, Buzás EI, Giricz Z. Isolation of high-purity extracellular vesicles by the combination of iodixanol density gradient ultracentrifugation and bind-elute chromatography from blood plasma. Front Physiol. 2018;9(OCT):1–11.
74. R Core Team. R: A Language and Environment for Statistical Computing [Internet]. Vienna, Austria; 2022. Available from: https://www.r-project.org/
75. Visnovitz T, Osteikoetxea X, Sódar BW, Mihály J, Lőrincz P, Vukman K V., Tóth EÁ, Koncz A, Székács I, Horváth R, Varga Z, Buzás EI. An improved 96 well plate format lipid quantification assay for standardisation of experiments with extracellular vesicles. J Extracell Vesicles. 2019;8(1).
76. Hutter JL, Bechhoefer J. Calibration of atomic-force microscope tips. Rev Sci Instrum. 1993;64(7):1868–1873.
77. LeClaire M, Gimzewski J, Sharma S. A review of the biomechanical properties of single extracellular vesicles. Nano Sel. 2021;2(1):1–15.
78. Bache N, Geyer PE, Bekker-Jensen DB, Hoerning O, Falkenby L, Treit P V., Doll S, Paron I, Müller JB, Meier F, Olsen J V., Vorm O, Mann M. A novel LC system embeds analytes in pre-formed gradients for rapid, ultra-robust proteomics. Mol Cell Proteomics. 2018;17(11):2284–2296.
79. Meier F, Brunner AD, Koch S, Koch H, Lubeck M, Krause M, Goedecke N, Decker J, Kosinski T, Park MA, Bache N, Hoerning O, Cox J, Räther O, Mann M. Online parallel accumulation–serial fragmentation (PASEF) with a novel trapped ion mobility mass spectrometer. Mol Cell Proteomics. 2018;17(12):2534–2545.
80. Perez-Riverol Y, Bai J, Bandla C, García-Seisdedos D, Hewapathirana S, Kamatchinathan S, Kundu DJ, Prakash A, Frericks-Zipper A, Eisenacher M, Walzer M, Wang S, Brazma A, Vizcaíno JA. The PRIDE database resources in 2022: A hub for mass spectrometry-based proteomics evidences. Nucleic Acids Res. 2022;50(D1):D543–552.
81. Cox J, Mann M. MaxQuant enables high peptide identification rates,

individualized p.p.b.-range mass accuracies and proteome-wide protein quantification. Nat Biotechnol. 2008;26(12):1367–1372.

82. Cox J, Hein MY, Luber CA, Paron I, Nagaraj N, Mann M. Accurate proteome-wide label-free quantification by delayed normalization and maximal peptide ratio extraction, termed MaxLFQ. Mol Cell Proteomics. 2014;13(9):2513–2526.
83. Tyanova S, and Cox J. Perseus: A Bioinformatics Platform for Integrative Analysis of Proteomics Data in Cancer Research. In: von Stechow L, editor. Cancer Systems Biology: Methods and Protocols [Internet]. "Springer New York; 2018. p. 133–148. Available from: https://doi.org/10.1007/978-1-4939-7493-1_7
84. Snel B, Lehmann G, Bork P, Huynen MA. String: A web-server to retrieve and display the repeatedly occurring neighbourhood of a gene. Nucleic Acids Res. 2000;28(18):3442–2444.
85. Szklarczyk D, Kirsch R, Koutrouli M, Nastou K, Mehryary F, Hachilif R, Gable AL, Fang T, Doncheva NT, Pyysalo S, Bork P, Jensen LJ, von Mering C. The STRING database in 2023: protein–protein association networks and functional enrichment analyses for any sequenced genome of interest. Nucleic Acids Res. 2023;51(D1):D638–646.
86. Schmittgen TD, Livak KJ. Analyzing real-time PCR data by the comparative CT method. Nat Protoc. 2008;3(6):1101–1108.
87. Schneider CA, Rasband WS, Eliceiri KW. NIH Image to ImageJ: 25 years of image analysis. Nat Methods. 2012;9(7):671–675.
88. Carpentier G, Martinelli M, Courty J, Cascone I. Angiogenesis Analyzer for ImageJ [Internet]. Available from: http://imagej.nih.gov/ij/macros/toolsets/Angiogenesis Analyzer.txt
89. Hadley Wickham. ggplot2: Elegant Graphics for Data Analysis [Internet]. Springer-Verlag New York; 2016. Available from: https://ggplot2.tidyverse.org
90. Khadka NK, Mortimer MF, Marosvari M, Timsina R, Mainali L. Membrane elasticity modulated by cholesterol in model of porcine eye lens-lipid membrane. Exp Eye Res. 2022;220(208):1–33.
91. Doole FT, Kumarage T, Ashkar R, Brown MF. Cholesterol Stiffening of Lipid Membranes. J Membr Biol [Internet]. 2022;255(4–5):385–405. Available from: https://doi.org/10.1007/s00232-022-00263-9

92. Chakraborty S, Doktorova M, Molugu TR, Heberle FA, Scott HL, Dzikovski B, Nagao M, Stingaciu LR, Standaert RF, Barrera FN, Katsaras J, Khelashvili G, Brown MF, Ashkar R. How cholesterol stiffens unsaturated lipid membranes. Proc Natl Acad Sci U S A. 2020;117(36):21896–21905.
93. Bairamukov V, Bukatin A, Landa S, Burdakov V, Shtam T, Chelnokova I, Fedorova N, Filatov M, Starodubtseva M. Biomechanical properties of blood plasma extracellular vesicles revealed by atomic force microscopy. Biology (Basel). 2021;10(1):1–10.
94. Liang X, Mao G, Ng KYS. Mechanical properties and stability measurement of cholesterol-containing liposome on mica by atomic force microscopy. J Colloid Interface Sci. 2004;278(1):53–62.
95. Liang X, Mao G, Ng KYS. Probing small unilamellar EggPC vesicles on mica surface by atomic force microscopy. Colloids Surfaces B Biointerfaces. 2004;34(1):41–51.
96. Vorselen D, van Dommelen SM, Sorkin R, Piontek MC, Schiller J, Döpp ST, Kooijmans SAA, van Oirschot BA, Versluijs BA, Bierings MB, van Wijk R, Schiffelers RM, Wuite GJL, Roos WH. The fluid membrane determines mechanics of erythrocyte extracellular vesicles and is softened in hereditary spherocytosis. Nat Commun [Internet]. 2018;9(1). Available from: http://dx.doi.org/10.1038/s41467-018-07445-x
97. Sakai-Kato K, Yoshida K, Takechi-Haraya Y, Izutsu KI. Physicochemical characterization of liposomes that mimic the lipid composition of exosomes for effective intracellular trafficking. Langmuir. 2020;36(42):12735–12744.
98. Ridolfi A, Brucale M, Montis C, Caselli L, Paolini L, Borup A, Boysen AT, Loria F, Van Herwijnen MJC, Kleinjan M, Nejsum P, Zarovni N, Wauben MHM, Berti D, Bergese P, Valle F. AFM-Based High-Throughput Nanomechanical Screening of Single Extracellular Vesicles. Anal Chem. 2020;92(15):10274–10282.
99. Bachurski D, Schuldner M, Nguyen PH, Malz A, Reiners KS, Grenzi PC, Babatz F, Schauss AC, Hansen HP, Hallek M, Pogge von Strandmann E. Extracellular vesicle measurements with nanoparticle tracking analysis–An accuracy and repeatability comparison between NanoSight NS300 and ZetaView. J Extracell Vesicles [Internet]. 2019;8(1). Available from:

https://doi.org/10.1080/20013078.2019.1596016

100. Fernandes-Alnemri T, Wu J, Yu JW, Datta P, Miller B, Jankowski W, Rosenberg S, Zhang J, Alnemri ES. The pyroptosome: A supramolecular assembly of ASC dimers mediating inflammatory cell death via caspase-1 activation. Cell Death Differ. 2007;14(9):1590–1604.
101. Kalra H, Simpson RJ, Ji H, Aikawa E, Altevogt P, Askenase P, Bond VC, Borràs FE, Breakefield X, Budnik V, Buzas E, Camussi G, Clayton A, Cocucci E, Falcon-Perez JM, Gabrielsson S, Gho YS, Gupta D, Harsha HC, Hendrix A, Hill AF, Inal JM, Jenster G, Krämer-Albers EM, Lim SK, Llorente A, Lötvall J, Marcilla A, Mincheva-Nilsson L, Nazarenko I, Nieuwland R, Nolte-'t Hoen ENM, Pandey A, Patel T, Piper MG, Pluchino S, Prasad TSK, Rajendran L, Raposo G, Record M, Reid GE, Sánchez-Madrid F, Schiffelers RM, Siljander P, Stensballe A, Stoorvogel W, Taylor D, Thery C, Valadi H, van Balkom BWM, Vázquez J, Vidal M, Wauben MHM, Yáñez-Mó M, Zoeller M, Mathivanan S. Vesiclepedia: A Compendium for Extracellular Vesicles with Continuous Community Annotation. PLoS Biol. 2012;10(12):8–12.
102. Pathan M, Fonseka P, Chitti S V., Kang T, Sanwlani R, Van Deun J, Hendrix A, Mathivanan S. Vesiclepedia 2019: A compendium of RNA, proteins, lipids and metabolites in extracellular vesicles. Nucleic Acids Res. 2019;47(D1):D516–519.
103. Hurley JH. The ESCRT Complexes. Crit Rev Biochem Mol Biol [Internet]. 2010;45(6):463–487. Available from: https://www.ncbi.nlm.nih.gov/pmc/articles/PMC3624763/pdf/nihms412728.pdf
104. Martins-Marques T, Costa MC, Catarino S, Simoes I, Aasen T, Enguita FJ, Girao H. Cx43-mediated sorting of miRNAs into extracellular vesicles. EMBO Rep. 2022;23(7):1–17.
105. Zhao S, Mi Y, Guan B, Zheng B, Wei P, Gu Y, Zhang Z, Cai S, Xu Y, Li X, He X, Zhong X, Li G, Chen Z, Li D. Tumor-derived exosomal miR-934 induces macrophage M2 polarization to promote liver metastasis of colorectal cancer. J Hematol Oncol. 2020;13(1):1–19.
106. Groot M, Lee H. Sorting Mechanisms for MicroRNAs into Extracellular Vesicles and Their Associated Diseases. Cells. 2020;9(4):1–16.
107. Chen C, Zheng H, Luo Y, Kong Y, An M, Li Y, He W, Gao B, Zhao Y, Huang H,

Huang J, Lin T. SUMOylation promotes extracellular vesicle-mediated transmission of lncRNA ELNAT1 and lymph node metastasis in bladder cancer. J Clin Invest. 2021;131(8):1–19.

108. Dou R, Liu K, Yang C, Zheng J, Shi D, Lin X, Wei C, Zhang C, Fang Y, Huang S, Song J, Wang S, Xiong B. EMT-cancer cells-derived exosomal miR-27b-3p promotes circulating tumour cells-mediated metastasis by modulating vascular permeability in colorectal cancer. Clin Transl Med. 2021;11(12).
109. Liu DW, Liu FX, Li ZY, Pan SK, Xie JW, Zhao ZH, Liu ZJ, Zhang JH, Liu ZS. HNRNPA1-mediated exosomal sorting of miR-483-5p out of renal tubular epithelial cells promotes the progression of diabetic nephropathy-induced renal interstitial fibrosis. Cell Death Dis [Internet]. 2021;12(3). Available from: http://dx.doi.org/10.1038/s41419-021-03460-x
110. Ramazani Y, Knops N, Elmonem MA, Nguyen TQ, Arcolino FO, van den Heuvel L, Levtchenko E, Kuypers D, Goldschmeding R. Connective tissue growth factor (CTGF) from basics to clinics. Matrix Biol [Internet]. 2018;68–69:44–66. Available from: https://doi.org/10.1016/j.matbio.2018.03.007
111. Luo Y, Li Z, Kong Y, He W, Zheng H, An M, Lin Y, Zhang D, Yang J, Zhao Y, Chen C, Chen R. KRAS mutant-driven SUMOylation controls extracellular vesicle transmission to trigger lymphangiogenesis in pancreatic cancer. J Clin Invest. 2022;132(14):1–19.
112. Campos A, Salomon C, Bustos R, Díaz J, Martínez S, Silva V, Reyes C, Díaz-Valdivia N, Varas-Godoy M, Lobos-González L, Quest AF. Caveolin-1-containing extracellular vesicles transport adhesion proteins and promote malignancy in breast cancer cell lines. Nanomedicine. 2018;13(20):2597–2609.
113. Cao YL, Zhuang T, Xing BH, Li N, Li Q. Exosomal DNMT1 mediates cisplatin resistance in ovarian cancer. Cell Biochem Funct. 2017;35(6):296–303.
114. Moon HG, Kim SH, Gao J, Quan T, Qin Z, Osorio JC, Rosas IO, Wu M, Tesfaigzi Y, Jin Y. CCN1 secretion and cleavage regulate the lung epithelial cell functions after cigarette smoke. Am J Physiol - Lung Cell Mol Physiol. 2014;307(4):326–337.
115. Kim AY, Park YJ, Pan X, Shin KC, Kwak SH, Bassas AF, Sallam RM, Park KS, Alfadda AA, Xu A, Kim JB. Obesity-induced DNA hypermethylation of the

adiponectin gene mediates insulin resistance. Nat Commun [Internet]. 2015;6(May):1–11. Available from: http://dx.doi.org/10.1038/ncomms8585

116. Yu CY, Theusch E, Lo K, Mangravite LM, Naidoo D, Kutilova M, Medina MW. HNRNPA1 regulates HMGCR alternative splicing and modulates cellular cholesterol metabolism. Hum Mol Genet. 2014;23(2):319–332.
117. Jiang S, Meng X, Gu H, Sun J, Chen S, Chen Z, Liu D, Liang X. STAU1 promotes adipogenesis by regulating the alternative splicing of Pparγ2 mRNA. Biochim Biophys Acta - Mol Cell Biol Lipids. 2023;1868(5):1–11.
118. Stadion M, Schwerbel K, Graja A, Baumeier C, Rödiger M, Jonas W, Wolfrum C, Staiger H, Fritsche A, Häring HU, Klöting N, Blüher M, Fischer-Posovszky P, Schulz TJ, Joost HG, Vogel H, Schürmann A. Increased Ifi202b/IFI16 expression stimulates adipogenesis in mice and humans. Diabetologia. 2018;61(5):1167–1179.
119. Théry C, Witwer KW, Aikawa E, Alcaraz MJ, Anderson JD, Andriantsitohaina R, Antoniou A, Arab T, Archer F, Atkin-smith GK, Ayre DC, Bach J marie, Bachurski D, Baharvand H, Balaj L, Baldacchino S, Bauer NN, Baxter AA, Bebawy M, Beckham C, Zavec AB, Benmoussa A, Berardi AC, Bergese P, Bielska E, Blenkiron C, Bobis-wozowicz S, Boilard E, Brisson A, Broekman MLD, Bromberg JF, Bryl-górecka P, Buch S, Buck AH, Burger D, Busatto S, Buschmann D, Bussolati B, Buzás EI, Byrd JB, Camussi G, Carter DRF, Caruso S, Chamley LW, Chang Y ting, Chaudhuri AD, Chen C. Minimal information for studies of extracellular vesicles 2018 (MISEV2018): a position statement of the International Society for Extracellular Vesicles and update of the MISEV2014 guidelines. 2018;7.
120. Blandin A, Dugail I, Hilairet G, Ponnaiah M, Ghesquière V, Froger J, Ducheix S, Fizanne L, Boursier J, Cariou B, Lhomme M, Le Lay S. Lipidomic analysis of adipose-derived extracellular vesicles reveals specific EV lipid sorting informative of the obesity metabolic state. Cell Rep. 2023;42(3).
121. Aswad H, Forterre A, Wiklander OPB, Vial G, Danty-Berger E, Jalabert A, Lamazière A, Meugnier E, Pesenti S, Ott C, Chikh K, El-Andaloussi S, Vidal H, Lefai E, Rieusset J, Rome S. Exosomes participate in the alteration of muscle homeostasis during lipid-induced insulin resistance in mice. Diabetologia.

2014;57(10):2155–2164.

122. Muraki R, Morita Y, Ida S, Kitajima R, Furuhashi S, Takeda M, Kikuchi H, Hiramatsu Y, Takanashi Y, Hamaya Y, Sugimoto K, Ito J, Kawata K, Kawasaki H, Sato T, Kahyo T, Setou M, Takeuchi H. Phosphatidylcholine in bile-derived small extracellular vesicles as a novel biomarker of cholangiocarcinoma. Cancer Med. 2023;(October 2022):1–12.
123. Jung JH, Lee MY, Choi DY, Lee JW, You S, Lee KY, Kim J, Kim KP. Phospholipids of tumor extracellular vesicles stratify gefitinib-resistant nonsmall cell lung cancer cells from gefitinib-sensitive cells. Proteomics. 2015;15(4):824–835.
124. Timmerman N, Waissi F, Dekker M, de Borst GJ, van Bennekom J, de Winter RJ, Hilvo M, Jylhä A, Pasterkamp G, de Kleijn DPV, Laaksonen R. Ceramides and phospholipids in plasma extracellular vesicles are associated with high risk of major cardiovascular events after carotid endarterectomy. Sci Rep [Internet]. 2022;12(1):1–13. Available from: https://doi.org/10.1038/s41598-022-09225-6
125. Strauss K, Goebel C, Runz H, Möbius W, Weiss S, Feussner I, Simons M, Schneider A. Exosome secretion ameliorates lysosomal storage of cholesterol in Niemann-Pick type C disease. J Biol Chem [Internet]. 2010 Aug 20 [cited 2020 Mar 3];285(34):26279–26288. Available from: http://dx.doi.org/10.1074/jbc.M110.134775
126. Lingwood D, Simons K. Lipid rafts as a membrane-organizing principle. Science (80-). 2010;327(5961):46–50.
127. Pollet H, Conrard L, Cloos AS, Tyteca D. Plasma membrane lipid domains as platforms for vesicle biogenesis and shedding? Vol. 8, Biomolecules. 2018.
128. Gan L, Liu D, Xie D, Lau WB, Liu J, Christopher TA, Lopez B, Liu L, Hu H, Yao P, He Y, Gao E, Koch WJ, Zhao J, Ma XL, Cao Y, Wang Y. Ischemic Heart-Derived Small Extracellular Vesicles Impair Adipocyte Function. Circ Res. 2022;130(1):48–66.
129. Crewe C, Funcke JB, Li S, Joffin N, Gliniak CM, Ghaben AL, An YA, Sadek HA, Gordillo R, Akgul Y, Chen S, Samovski D, Fischer-Posovszky P, Kusminski CM, Klein S, Scherer PE. Extracellular vesicle-based interorgan transport of mitochondria from energetically stressed adipocytes. Cell Metab.

2021;33(9):1853-1868.

130. Kita S, Maeda N, Shimomura I. Interorgan communication by exosomes, adipose tissue, and adiponectin in metabolic syndrome. J Clin Invest. 2019;129(10):4041–4049.

131. Li W, Li Y, Zhi W, Liu C, Fan W, Miao Q, Gu X. Diagnostic value of using exosome-derived cysteine-rich protein 61 as biomarkers for acute coronary syndrome. Exp Ther Med. 2021;22(6).

132. Martins-Marques T, Ribeiro-Rodrigues T, de Jager SC, Zuzarte M, Ferreira C, Cruz P, Reis L, Baptista R, Gonçalves L, Sluijter JPG, Girao H. Myocardial infarction affects Cx43 content of extracellular vesicles secreted by cardiomyocytes. Life Sci Alliance. 2020;3(12):1–16.

133. Smit KF, Konkel M, Kerindongo R, Landau MA, Zuurbier CJ, Hollmann MW, Preckel B, Nieuwland R, Albrecht M, Weber NC. Helium alters the cytoskeleton and decreases permeability in endothelial cells cultured in vitro through a pathway involving Caveolin-1. Sci Rep [Internet]. 2018;8(1):1–12. Available from: http://dx.doi.org/10.1038/s41598-018-23030-0

9 Bibliography of the candidate's publications

1. Chen S, Wang Q, Bakker D, Hu X, Zhang L, van der Made I, Tebbens AM, Kovácsházi C, Giricz Z, Brenner GB, Ferdinandy P, Schaart G, Gemmink A, Hesselink MKC, Ribadu MR, Pieper MP, Hollmann MW, Weber NC, Balligand JL, Creemers EE, Coronel R, Zuurbier CJ. Empagliflozin prevents heart failure through inhibition of the NHE1-NO pathway, independent of SGLT2. Basic Res Cardiol [Internet]. 2024;(0123456789). Available from: https://doi.org/10.1007/s00395-024-01067-9
2. Kovácsházi C, Hambalkó S, Sayour N V, Gergely TG, Brenner GB, Pelyhe C, Kapui D, Weber BY, Hültenschmidt AL, Pállinger É, Buzás EI, Zolcsák Á, Kiss B, Bozó T, Csányi C, Kósa N, Kellermayer M, Farkas R, Karvaly GB, Wynne K, Matallanas D, Ferdinandy P. Effect of hypercholesterolemia on circulating and cardiomyocyte - derived extracellular vesicles. Sci Rep [Internet]. 2024;1–14. Available from: https://doi.org/10.1038/s41598-024-62689-6
3. Sundaramurthi H, Tonelotto V, Wynne K, O'Connell F, O'Reilly E, Costa-Garcia M, Kovácsházi C, Kittel A, Marcone S, Blanco A, Pallinger E, Hambalkó S, Piulats Rodriguez JM, Ferdinandy P, O'Sullivan J, Matallanas D, Jensen LD, Giricz Z, Kennedy BN. Ergolide mediates anti-cancer effects on metastatic uveal melanoma cells and modulates their cellular and extracellular vesicle proteomes. Open Res Eur. 2023;3:1–24.
4. Sayour N V., Brenner GB, Makkos A, Kiss B, Kovácsházi C, Gergely TG, Aukrust SG, Tian H, Zenkl V, Gömöri K, Szabados T, Bencsik P, Heinen A, Schulz R, Baxter GF, Zuurbier CJ, Vokó Z, Ferdinandy P, Giricz Z. Cardioprotective efficacy of limb remote ischaemic preconditioning in rats: discrepancy between a meta-analysis and a three-centre in vivo study. Cardiovasc Res [Internet]. 2023;119(6):1336–1351. Available from: https://doi.org/10.1093/cvr/cvad024
5. Gergely TG, Brenner GB, Nagy RN, Sayour N V., Makkos A, Kovácsházi C, Tian H, Schulz R, Giricz Z, Görbe A, Ferdinandy P. Effects of Bempedoic Acid in Acute Myocardial Infarction in Rats: No Cardioprotection and No Hidden Cardiotoxicity. Int J Mol Sci. 2023;24(2).
6. Hegyesi H, Pallinger É, Mecsei S, Hornyák B, Kovácsházi C, Brenner GB, Giricz Z, Pálóczi K, Kittel Á, Tóvári J, Turiak L, Khamari D, Ferdinandy P, Buzás EI.

Circulating cardiomyocyte-derived extracellular vesicles reflect cardiac injury during systemic inflammatory response syndrome in mice. Cell Mol Life Sci [Internet]. 2022;79(2):1–15. Available from: https://doi.org/10.1007/s00018-021-04125-w

7. Jelemenský M, Kovácsházi C, Ferenczyová K, Hofbauerová M, Kiss B, Pállinger É, Kittel Á, Sayour VN, Görbe A, Pelyhe C, Hambalkó S, Kindernay L, Barančík M, Ferdinandy P, Barteková M, Giricz Z. Helium conditioning increases cardiac fibroblast migration which effect is not propagated via soluble factors or extracellular vesicles. Int J Mol Sci. 2021;22(19).
8. Pajović V, Kovácsházi C, Kosić M, Vasić M, Đukić L, Brenner GB, Giricz Z, Bajić D, Ferdinandy P, Japundžić-Žigon N. Phenomapping for classification of doxorubicin-induced cardiomyopathy in rats. Toxicol Appl Pharmacol. 2021;423(May).
9. Madonna R, Guarnieri S, Kovácsházi C, Görbe A, Giricz Z, Geng YJ, Mariggiò MA, Ferdinandy P, De Caterina R. Telomerase/myocardin expressing mesenchymal cells induce survival and cardiovascular markers in cardiac stromal cells undergoing ischaemia/reperfusion. J Cell Mol Med. 2021;25(12):5381–5390.
10. Póti Á, Gyergyák H, Németh E, Rusz O, Tóth S, Kovácsházi C, Chen D, Szikriszt B, Spisák S, Takeda S, Szakács G, Szallasi Z, Richardson AL, Szüts D. Correlation of homologous recombination deficiency induced mutational signatures with sensitivity to PARP inhibitors and cytotoxic agents. Genome Biol. 2019;20(1):1–13.

10 Acknowledgements

Hereby I want to express my gratitude to all those who have supported me over the past five years in my research and beyond.

First of all, I am deeply thankful to my parents for their dedicated support throughout my studies and for always expressing how proud they are of me.

I am profoundly grateful to my wife Fruzsina, for her infinite support in my life, including my scientific career. I specially thank that she has willingly stayed alone with the kids during my long absences for conferences.

I owe a special debt of gratitude to my supervisor, dr. Zoltán Giricz, without whom this thesis would not have been possible. His guidance and the knowledge he imparted over the last five years have been crucial to my progress. I also want to thank prof. dr. Péter Ferdinandy for his financial support and expert advice, which have greatly facilitated our research.

I am grateful to all the senior PhDs who assisted me during my studies, particularly dr. Gábor Brenner, dr. András Makkos, dr. Zsófia Gulyás-Onódi and dr. Viktória Tóth. They were always willing to help with any technical questions and difficulties I encountered.

I must also thank all room members of the 406 PdF room for creating an uplifting environment, making our workspace a pleasant and motivating place.

Finally, I want to thank God that I can work as a researcher with such excellent people. I am grateful for the skills and energy He has given me to reach this far and complete my PhD thesis.